Nanoscale Horizons

ROYAL SOCIETY OF CHEMISTRY

COMMUNICATION

View Article Online
View Journal | View Issue

Check for updates

Cite this: *Nanoscale Horiz.*, 2025, **10**, 2550

Received 1st May 2025,
Accepted 18th July 2025

DOI: 10.1039/d5nh00299k

rsc.li/nanoscale-horizons

A modular polymer platform for efficient mRNA delivery in cancer immunotherapy

Guanyou Lin,† Jianxi Huang,† Xinqi Li, Yunshan Liu, Taylor Juenke, Arthur Finstad and Miqin Zhang *

Department of Materials Science and Engineering, University of Washington, Seattle, Washington 98195, USA. E-mail: mzhang@uw.edu

† These authors contributed equally.

The use of mRNA for prophylactic and therapeutic applications, such as treating coronavirus and cancer, has garnered significant attention. However, owing to the inherent labile nature of mRNA, it requires robust delivery platforms to enable effective mRNA-based therapies. While lipid nanoparticles (LNPs) have shown success in mRNA delivery, they face challenges in terms of safety, storage and manufacturing costs. Polymeric mRNA delivery platforms have emerged as promising alternatives due to their structural versatility, durability, and transfection efficiency. This study presents PFHA-PEI-mRNA-HP, a polymeric mRNA delivery nanoplatform that utilizes simultaneous fluorination and heparinization of low molecular weight polyethylenimine (PEI)-based mRNA complexes to enhance performance. These modifications applied to the PEI backbone significantly improved the physicochemical properties, cellular uptake, endosomal escape capability, and biocompatibility of the platform, resulting in a substantial increase in transfection efficiency. PFHA-PEI-mRNA-HP achieved ultra-high transfection efficiency of >90% across multiple cancer cell types, outperforming the LNP-based delivery reagent Lipofectamine 2000. Additionally, PFHA-PEI-mRNA-HP demonstrated superior stability compared to Lipofectamine 2000 when stored above 0 °C for 15 days. When loaded with therapeutic IL12 mRNA, PFHA-PEI-mRNA-HP effectively delivered its payload *in vivo* and, in combination with anti-PD-L1 therapy, significantly inhibited tumor growth in a triple-negative breast cancer mouse model without causing harm to healthy tissues. These results highlight PFHA-PEI-mRNA-HP as a highly efficient and reliable mRNA delivery platform for cancer gene therapies.

New concepts

This research presents an innovative polymeric mRNA delivery platform that addresses key limitations of lipid nanoparticles (LNPs) widely used in mRNA therapeutics. Despite their clinical success, LNPs rely on complex multicomponent lipid formulations, labor-intensive screening, and cold-chain storage, resulting in batch inconsistencies and high costs. Furthermore, their limited lipid reactive sites restrict functionalization for targeted therapies. PFHA-PEI-mRNA-HP, based on a single, fluorinated, and heparinized low molecular weight PEI macromolecule, forms cationic nanoparticles that self-assemble with mRNA *via* simple mixing, enhancing scalability, affordability, and consistency. Fluorination boosts cellular uptake and endosomal escape, while heparinization improves biocompatibility and stability. This platform outperforms Lipofectamine 2000 in terms of transfection efficiency across different cancer cell lines and remains stable without cold storage. *In vivo*, it effectively delivers IL12 mRNA, suppressing triple-negative breast cancer in mice alongside anti-PD-L1 therapy without toxicity. This study not only provides insights into designing and optimizing a novel polymeric mRNA delivery platform but also conceptually demonstrates the promising utility of functionalized cationic polymers in the field of mRNA delivery.

Miqin Zhang

Congratulations to Nanoscale Horizons on a decade of excellence in nanoscience and technology! The Journal has consistently showcased high-quality and innovative research that advances the frontiers of the field. It was a great honor to serve on the editorial board from 2018 to 2024. We are excited to share our recent work on a polymeric nanoplatform that tackles key challenges in mRNA delivery, offering design insights and highlighting the therapeutic potential of functionalized cationic polymers. Here's to another decade as a leading platform for groundbreaking discoveries in nanoscience and materials-based medicine.

1. Introduction

Messenger RNA (mRNA), the intermediator between the fixed genetic blueprint (DNA) and the terminal effector (proteins),

offers great flexibility and utility as a medicinal agent.[1] The delivery of prophylactic mRNA payloads *via* nanomaterial-based platforms has shown technological prowess in addressing the significant public health challenges faced worldwide during the recent pandemic years. Successful mRNA transfection can express virtually any proteins of design in cells and tissues to manipulate cell behaviors and exert prophylactic or therapeutic effects to treat or prevent diseases. The cytosolic mRNA activity, which eliminates the need to pass the nuclear envelope barrier of the cell for transient protein expression and the risk of insertional mutagenesis, enables facile and safe transfection.[2] However, due to the labile nature of mRNA, the main challenge of mRNA delivery is finding a reliable carrier offering protection from enzymatic and chemical degradation while ferrying mRNA across biological barriers. While lipid nanoparticles (LNPs) have achieved remarkable success as an mRNA delivery platform for vaccines and treatments, there is still room for improvement to address the safety concerns associated with LNP-mRNA formulations. These formulations may pose limitations and potential side effects when applied clinically.[3–5] Recent findings also pointed out that LNPs not only encapsulate mRNA but also water pockets, which could readily subject mRNA to hydrolysis and jeopardize its structural integrity unless stored under ultra-cold conditions (−20 °C to −80 °C).[6–8] The manufacture of LNP-mRNA requires meticulous mixing of many different lipid constituents (usually four) with mRNA in aqueous-organic solvent mixtures, commonly using water-ethanol, in high precision mixing platforms, such as rapid microfluidic mixing devices, to ensure reproducibility.[9,10] To equip LNPs with active tumor targeting ability, additional reactive lipids need to be added to them for post-synthetic ligand installation, which could further complicate the manufacture process of LNPs and alter their structural integrity, which is largely based on weak electrostatic and hydrophobic interactions.[11] Therefore, it is necessary to develop a novel class of mRNA delivery platforms that can build on the success of LNPs, while addressing their limitations. Efforts to modify LNPs with polymeric moieties to improve their mRNA delivery performance have been reported in recent years.[12,13]

Cationic polymer-based mRNA delivery platforms have also gained extensive research recognition. Different from LNPs, a cationic polymer can be simultaneously equipped with multiple functional moieties so that only very few polymeric constituents are needed to form nanoparticles (NPs) with mRNA, making the production of polymeric mRNA NPs much easier and less costly than that of LNP-mRNA.[10] Also, due to their larger-than-lipid molecular weight and abundant in positive charge, cationic polymers can form more robust and stable complexes with mRNA which can better protect mRNA from degradation than lipids *via* multivalent electrostatic condensation.[14] Among the numerous types of cationic polymers, only polyethyleneimine (PEI) is widely applied to deliver mRNA due to its superior capability of mRNA condensation and endosomal escape.[15] To circumvent the non-biodegradability and cytotoxicity issues of large molecular weight PEI, low molecular weight branched PEI-based delivery platforms have been developed, showing great efficacy in delivering mRNA for vaccination against HIV and influenza viruses as well as treating muscle dystrophy. This demonstrates the utility and suitability of low molecular weight branched PEI for mRNA delivery applications.[16–19] However, the mRNA transfection efficiency of these mRNA delivery platforms was either inferior to that of LNPs or only comparable to that of the toxic high molecular weight PEI, leaving the transfection efficiency of low molecular weight PEI-based mRNA delivery platforms still in doubt.

Fluorine has been widely utilized in the medicinal industry to modify the molecular structures of drugs for better pharmacokinetic and therapeutic outcomes and imaging applications.[20–23] In the context of biomaterials, fluorination, which is typically achieved by incorporating fluorocarbon moieties into polymer structures, has recently been shown to substantially improve the gene delivery efficiency of cationic polymers.[24–27] This enhancement arises from several key properties of fluorocarbons. Firstly, fluorinated chains exhibit amphiphobicity, they are both hydrophobic and lipophobic, leading to low interfacial energy and reduced nonspecific interactions with proteins and membranes.[28,29] Secondly, fluorocarbon-modified polymers have a strong tendency to self-assemble into compact and stable nanostructures, which improves the condensation of mRNA and protects it from enzymatic degradation.[30] Thirdly, fluorinated polymers facilitate crossing biological barriers, such as the plasma membrane and endosomal compartments, by promoting membrane destabilization and escape.[31–33] These combined effects, including enhanced stability, reduced non-specific adsorption, and improved intracellular trafficking, make fluorinated cationic polyplexes promising carriers for nucleic acid delivery. Fluorinated cationic polyplexes have been reported to have high efficiency in delivering DNA,[24,25] siRNA[34,35] and proteins[36] but have been rarely reported for mRNA delivery.

A common dilemma in polymeric gene delivery platforms is that the high density of cationic charges necessary for effective nucleic acid condensation also poses the issues of toxicity, insufficient nucleic acid release and serum protein adsorption. A promising solution for these problems is embellishing cationic polyplexes with polyanions. Adding polyanions not only improves the biocompatibility and serum stability of complexes by partially shielding their positive surface charge but also helps tune the binding tightness between cationic polymers and nucleic acids, thus achieving a subtle packing-unpacking balance for efficient nucleic acid release.[37,38] As a biocompatible polysaccharide with high anionic charge density, heparin (HP) has been repeatedly reported to significantly improve the biocompatibility, nucleic acid release profile and transfection efficiency of various types of cationic polyplexes when incorporated in them.[39–41] Although the polyanion embellishment strategy has been proven to be effective for DNA and RNAi delivery, whether the same strategy would display a similar enhancement effect on mRNA delivery platforms remains largely unexplored, if not completely unknown.

By combining the merits of low molecular weight branched PEI, fluorination, and heparin embellishment, polymeric mRNA

NP could yield a comparable or even better mRNA delivery efficiency than LNPs, while possessing superior structural integrity compatible with post-synthetic modifications such as targeting ligand conjugation, more robust storage stability, and simplified yet reproducible manufacture process. To this end, we introduced a polymeric NP mRNA delivery platform (termed PFHA-PEI-mRNA-HP) and demonstrated its utility in the transfection of multiple cancer types. Branched PEI with a molecular weight of 2 kDa, perfluoroheptanoic acid (PFHA) as the fluorocarbon moiety, and low molecular weight (1.8–7.5 kDa) heparin (HP) were selected as the constituents of this mRNA delivery platform. PFHA-PEI-mRNA-HP possessed a sub-hundred nm size, spherical shape and sufficient positive surface charge, which are conducive for effective mRNA delivery. Since the capability of achieving successful gene delivery in cancer cells is crucial in improving the therapeutic outcomes of cancer treatments, PFHA-PEI-mRNA-HP was applied to different types of cancer cells to test its *in vitro* mRNA delivery utility. Breast and liver cancer cells were chosen as the target cells given that they are the major types of cancers inflicting a large number of deaths worldwide (over 1.5 million in 2020).[42] Brain cancer cells were also tested because brain cancer is one the deadliest cancer types with a 5-year survival rate below 5% even though it is not as prevalent as breast and liver cancers.[43]

Notably, PFHA-PEI-mRNA-HP was able to achieve an ultra-high mRNA transfection efficiency ($>90\%$) across breast cancer cells, brain cancer cells and liver cancer cells, while showing innocuous toxicity profiles on these cell lines. PFHA-PEI-mRNA-HP exhibited superior stability to Lipofectamine 2000-mRNA LNP when stored at 4 °C for 15 days. Loaded with immunotherapeutic interleukin 12 (IL12) mRNA, PFHA-PEI-mRNA-HP demonstrated promising utility in inducing antitumor immunity to suppress the growth of metastatic triple negative breast cancer (TNBC) tumors *in vivo*, without causing harm to healthy tissues. The mRNA delivery performance and storage stability of PFHA-PEI-mRNA-HP demonstrated that it can be a highly efficient and reliable mRNA delivery platform for gene therapy against aggressive solid tumors and other diseases.

2. Materials and methods

2.1 Materials

CleanCap® EGFP mRNA was purchased from TriLink Biotechnologies (San Diego, CA, USA). Low molecular weight heparin was purchased from Galen Laboratory Supplies (North Haven, CT, USA). Branched PEI (MW 2 kDa) was purchased from Polysciences (Warrington, PA, USA). Microliter syringes (100 μL max volume) and removable needles (32 gauge, point style 3) were purchased from Hamilton (Reno, NV, USA). An NE-300 "Just Infusion"™ Syringe Pump was purchased from New Era Pump System Inc. (Farmingdale, NY, USA). (1-Ethyl-3-[3-dimethylaminopropyl]carbodiimide hydrochloride) (EDC), *N*-hydroxysuccinimide (NHS), Lab-Tek™ II 8-well chambered cover glass, NucBlue DAPI reagent, Lipofectamine 2000, LysoTracker™ Red DND-99, ultrapure agarose, antibiotic–antimycotic (100×), TrypLE Express Enzyme solution, RPMI 1640 and DMEM cell culture medium were purchased from Invitrogen (Carlsbad, CA, USA). HyClone characterized fetal bovine serum (FBS) was purchased from GE Healthcare Life Sciences (Pittsburgh, PA, USA). Label IT Tracker Intracellular Nucleic Acid Labeling Kits were purchased from Mirus Bio (Madison, WI, USA). Single Strand RNA ladder was purchased from New England Biolabs (Ipswich, MA, USA). SpectraPOR7 dialysis membrane was purchased from Repligen Corp (Waltham, MA, USA). Calcein AM Viability dye and propidium iodide were purchased from ThermoFisher Scientific (Waltham, MA, USA). All other chemicals were purchased from Sigma-Aldrich (St Louis, MO, USA). The 4T1, HepG2, MCF7, SF763 and C6 cell lines were purchased from American Type Culture Collection (Manassas, VA, USA). The M6 cell line was kindly shared by the Disis group from the Cancer Vaccine Institute at UW Medicine. IL12 DNA (Tandem p40p35) was a gift from Nevil Singh (Addgene plasmid # 108665).

2.2 Synthesis of PFHA-PEI

PFHA was conjugated onto PEI *via* EDC/NHS coupling chemistry. 127.4 mg of PFHA, 80.5 mg of EDC and 58.1 mg of NHS were separately dissolved in methanol at a concentration of 50 mg mL^{-1}. The PFHA, EDC and NHS solutions were mixed by adding EDC, and subsequently NHS to the PFHA solution. The mixed solution was placed on a rocker and incubated for 3 h at room temperature. Next, 100 mg branched PEI was dissolved in methanol at 50 mg mL^{-1} and added to the PFHA-EDC-NHS mixture solution and shaken at room temperature for 16 h. The resultant solution was dialyzed against Milli-Q water for 2 days using a 1k MWCO SpectraPOR7 dialysis membrane. The dialyzed solution was centrifuged at 4000 G for 5 min to precipitate out large aggregates. Then, the clear supernatant was freeze-dried and stored at −20 °C for long-term storage. The typical yield of a PFHA-PEI batch was around 60% of the combined mass of all the reactants.

2.3 FTIR spectra collection

2 mg of each of the PFHA, PEI and PFHA-PEI dry samples was mixed with 200 mg of KBr and pulverized into fine powders, and a pellet was prepared for characterization. FTIR spectra were obtained using a Nicolet 5-DXB FTIR spectrometer (ThermoFisher, Boston, MA) with a resolution of 4 cm^{-1} and average of 64 runs.

2.4 XPS spectral analysis

X-ray photoelectron spectroscopy (XPS, AXIS Ultra DLD/Surface Science Instruments S-Probe, Kratos) was performed to study the formation of the amide group (O═C–NH–). This instrument has a monochromatized Al Kα X-ray source and a low-energy electron flood gun for charge neutralization. The X-ray spot size for these acquisitions was in the order of 700 × 300 μm. An electrostatic lens was used for data collection. The pressure in the analytical chamber during spectral acquisition was less than 5×10^{-9} torr. The pass energy for the survey spectra (composition) was 160 eV. The pass energy for the high-resolution spectra was 40 eV. The take-off angle (the angle

between the sample normal and the input axis of the energy analyzer) was 0° (0-degree take-off angle ~100 Å sampling depth). The Kratos Vision2 software was used to determine the peak areas and calculate the elemental compositions from the peak areas. CasaXPS was used to fit the peaks in the high-resolution spectra. In the case of the high-resolution spectra, a Shirley background was used, and all binding energies were referenced to the C ls C–C bonds at 285.0 eV.

2.5 Formation of PFHA-PEI-mRNA-HP complex

PFHA-PEI was redissolved in Milli-Q water at 10 mg mL^{-1} and was centrifuged at 16 000 G for 10 min to eliminate possible large aggregates. The supernatant from PFHA-PEI was diluted to 7.5 mg mL^{-1} with 20 mM HEPES buffer (pH 7.4). mRNA was diluted to 0.5 mg mL^{-1} in 20 mM HEPES buffer (pH 7.4). HP was dissolved in 20 mM HEPES buffer (pH 7.4) at concentration of 0.5 mg mL^{-1}. To prepare the PFHA-PEI-mRNA complex, 5 μL of mRNA solution was mixed with 5 μL of PFHA-PEI solution *via* an RSM device. Specifically, 5 μL of PFHA-PEI solution was first added to the bottom of a 0.6 mL microtube and 5 μL of mRNA solution was loaded into a Hamilton microliter syringe. The mRNA solution was then slowly injected into the PFHA-PEI solution at a flow rate of 1 μL s^{-1} controlled by a syringe pump, while the PFHA-PEI solution was stirred by a rotor tip at 500 RPM to ensure homogenous mixing. To add HP to the PFHA-PEI-mRNA complex, the desired amount of HP was loaded into a Hamilton microliter syringe and slowly injected into the PFHA-PEI-mRNA solution at a flow rate of 0.5 μL s^{-1} controlled by a syringe pump, while the PFHA-PEI-mRNA solution was stirred by a rotor tip at 500 RPM to ensure homogenous mixing. To prepare the PEI-mRNA complex, PEI was first dissolved in 20 mM HEPES buffer (pH 7.4) at a concentration of 7.5 mg mL^{-1}, followed by the same mixing procedure as that for the preparation of the PFHA-PEI-mRNA complex.

2.6 Hydrodynamic size, serum stability and zeta potential measurement

The hydrodynamic size and zeta potential of PEI-mRNA, PFHA-PEI-mRNA and PFHA-PEI-mRNA-HP (with varying HP amounts) were determined using a Zetasizer Nano-ZS (Malvern Instruments, Worcestershire, UK). The measurements were performed in 20 mM HEPES buffer (pH 7.4) at room temperature. To test the serum stability of the samples, they were diluted 100 times with PBS supplemented with 10% fetal bovine serum (FBS) and placed in a 37 °C water bath. Hydrodynamic size measurements were performed at various time points within 3 weeks.

2.7 Gel electrophoresis retardation assay

Free mRNA, PEI-mRNA, PFHA-PEI-mRNA and PFHA-PEI-mRNA-HP (with varying HP amounts) samples were added to 1% agarose gel at 1 μg mRNA per lane. Gel electrophoresis was run for about 30 min at 120 V. Gels were stained with 0.5 μg mL^{-1} ethidium bromide and visualized using a Bio-Rad Universal Hood II Gel Doc System.

2.8 TEM imaging

TEM samples were prepared by the addition of 4 μL of PEI-mRNA, PFHA-PEI-mRNA or PFHA-PEI-mRNA-HP (with varying HP amounts) solution to a Formvar/carbon coated 300-mesh copper grid (Ted Pella, Inc., Redding, CA) and stained with 1% uranyl acetate, and subsequently allowed to air dry. TEM images were acquired on a Tecnai G2 F20 electron microscope (FEI, Hillsboro, OR) operating at a voltage of 200 kV.

2.9 Cell culture

4T1 and M6 mouse breast cancer cells were cultured in RPMI1640 medium supplemented with 10% vol/vol FBS and 1% vol/vol antibiotic–antimycotic. MCF7 human breast cancer cells, HepG2 human liver cancer cells, SF763 human glioblastoma cells and C6 rat glioma cells were cultured in DMEM medium supplemented with 10% vol/vol FBS and 1% vol/vol antibiotic–antimycotic. Culture media were replenished once every three days if the cells were not confluent enough to be passaged. When the cell density reached 80%, the 4T1, MCF7, HepG2, SF763 and C6 cells were dissociated with TrypLE agent and M6 with PBS + 2.5% v/v EDTA. Dissociated cells were suspended in their corresponding culture media and pelleted at 500 G for 5 min. Then, the desired number of cells was transferred to new culture flasks with fresh culture media. Cultures were maintained in a 37 °C and 5% CO_2 humidified incubator.

2.10 Cellular uptake and endosomal escape studies

mRNA was labeled with Cy5 following the manufacturer's protocol of the Label IT Tracker Intracellular Nucleic Acid Labeling Kit before complexed into PEI-mRNA, PFHA-PEI-mRNA and PFHA-PEI-mRNA-HP. 4T1, M6 and HepG2 cells were seeded at 15 000 cells per well in 8-well glass chambers. All cells were incubated for 24 h before treatments were added. Then, PEI-mRNA, PFHA-PEI-mRNA and PFHA-PEI-mRNA-HP were added to the cells at 2 μg mL^{-1} mRNA concentration, incubated for either 2 h or 12 h before adding 75 nM of LysoTracker Red DND reagent, and then incubated for another 1 h. There were two identical sets of samples for the 12-h time point experiment, where one set was incubated normally in a 37 °C incubator, while another set was incubated in a refrigerator at 4 °C. The refrigerated sample was briefly placed at room temperature for adding LysoTracker reagent and was immediately returned to 4 °C for 1 h incubation. Then, all cells were washed three times with cold PBS and fixed with paraformaldehyde (4% in PBS) for 15 min at room temperature. The fixed cells were further washed with cold PBS three times. NucBlue Fixed Cell ReadyProbes DAPI reagent was diluted 10 times in cold PBS and 100 μL was added to each well. Confocal images were acquired using a Leica SP8X confocal laser scanning microscope (Leica, Germany).

2.11 *In vitro* cell transfection

4T1, M6 and C6 cells were seeded at 4000 cells per well in 96-well plates. MCF7, HepG2 and SF763 were seeded at 8000 cells per well

in 96-well plates. All cells were incubated for 24 h after seeded on plates before treatments were added. PEI-mRNA, PFHA-PEI-mRNA, PFHA-PEI-mRNA-HP or Lipofectamine 2000-mRNA complexes were added to 100 μL of fully supplemented culture medium to give a final mRNA concentration of 2 μg mL^{-1} in each well for all cancer cell lines. The cells were incubated with the complexes for 48 h and the cell culture media were replenished after 24 h. For the FGFR inhibition study, the cells in the treatment group were pre-incubated with 500 nM PD173074 (FGFR inhibitor, ≥99% purity, purchased from Fisher Scientific, Cat# 506911) for 1 h prior to transfection. The inhibitor remained in the medium throughout the 48 h transfection period. Transfection using the commercial agent, Lipofectamine 2000, was performed following the manufacturer's protocol. The cells were imaged 48 h post-transfection with a Nikon TE300 inverted fluorescence microscope (Nikon, Tokyo, Japan).

2.12 Quantitative analysis of transfection *via* flow cytometry

After the cells were transfected following the *in vitro* cell transfection procedures, 40 μL TrypLE was added to each well and the wells were incubated for 8 min to dissociate adherent cells. Then, 100 μL cold PBS was added to the trypsinized wells to resuspend cells. The cell suspension was collected in 1.5 mL microtubes and centrifuged at 4 °C at 500 G for 5 min to pellet the cells. Then, the cell pellets were then resuspended in 200 μL cold PBS and transferred to flow cytometry tubes for immediate flow cytometry analysis on a FACSCanto II (BD Biosciences), from which the data was post-processed using the FlowJo software (Treestar, Inc., San Carlos, CA).

2.13 *In vitro* cell viability studies

4T1, M6 and HepG2 cells were seeded at 4000, 4000, 8000 cells per well in 96-well plates, respectively. All cells were incubated for 24 h after seeded on plates before treatments were added. Then, the cells were treated with PEI-mRNA, PFHA-PEI-mRNA, PFHA-PEI-mRNA-HP or Lipofectamine 2000-mRNA at mRNA concentrations of 0, 0.5, 1, 2, and 3 μg mL^{-1}. The cells were treated for 24 h before the cell viability was determined using the Alamar Blue assay. The fluorescent signal readout was obtained using a SpectraMax i3 microplate reader (Molecular Devices, Sunnyvale, CA, USA) with 550 nm excitation and 590 nm emission. The fluorescence intensities of all the treatment groups were normalized so that the viability of the untreated cell group was 100%.

2.14 Functionality test after storage above 0 °C

The PFHA-PEI-mRNA-HP and Lipofectamine 2000-mRNA complexes were prepared on day 0 and stored at 4 °C throughout this study. 4T1 and HepG2 cells were seeded at 4000 and 12 000 cells per well in 96-well plates, respectively. All cells were incubated for 24 h after seeded on plates before the treatments were added. PFHA-PEI-mRNA-HP and Lipofectamine 2000-mRNA complexes were added to 100 μL of fully supplemented culture media to give a final mRNA concentration of 2 μg mL^{-1} in each well on day 0, 1, 2, 3, 4, 7, and 15 after sample preparation. The cells were incubated with the complexes for 24 h before imaging with a Nikon TE300 inverted fluorescent microscope (Nikon, Tokyo, Japan).

2.15 *In vitro* transfection of IL12 mRNA

IL12 mRNA was synthesized from mouse IL12-encoding plasmid DNA obtained from Addgene (Plasmid #108665). The plasmid DNA was transcribed using the HiScribe® T7 ARCA mRNA Kit (New England Biolabs Inc, Ipswich, MA), and then purified with the Monarch RNA cleanup kit (New England Biolabs Inc, Ipswich, MA). To evaluate the transfection efficiency of PFHA-PEI-mRNA-HP for IL12 mRNA delivery, 4T1 cells were seeded in a 96-well plate at a density of 4×10^3 cells per well and incubated at 37 °C with 5% CO_2 overnight. The, the cells were transfected with PFHA-PEI-mRNA-HP complexes loaded with IL12 mRNA, following the same transfection protocol described in Section 2.11. At 2/12/24 h post-transfection, the cells were processed for immunofluorescence staining to visualize IL12 protein expression. For immunostaining, the culture medium was aspirated, and the cells were washed with 200 μL of phosphate-buffered saline (PBS) per well. The cells were fixed with 100 μL of 4% paraformaldehyde (PFA) for 10 min at room temperature, followed by additional washing with PBS. To allow intracellular staining, the cells were incubated with 100 μL of 1× intracellular staining permeabilization wash buffer (BioLegend, Cat. No. 421002) for 10 min at room temperature. After washing with PBS, 100 μL of PE-conjugated anti-mouse IL12 antibody (2 μg mL^{-1} in PBS) was added to each well, and the plate was incubated at 4 °C for 30 min. The cells were washed twice, followed by the addition of 100 μL of NucBlue® DAPI reagent (diluted 1 : 10 in PBS) to stain their nuclei. The plate was stored at 4 °C and protected from light until imaging. Fluorescence imaging was performed using a Nikon TE300 inverted fluorescence microscope (Tokyo, Japan). IL12 expression was detected using the PE channel, and cell nuclei were visualized in the DAPI channel.

2.16 *In vivo* therapeutic efficacy and biosafety profile studies of PFHA-PEI-mRNA-HP

All animal studies were conducted in compliance with institutional guidelines and approved by the Institutional Animal Care and Use Committee (IACUC). Female BALB/c mice (6–8 weeks old) were used to establish the 4T1 triple-negative breast cancer (TNBC) model. A total of 4.75×10^5 4T1 cells were resuspended in phosphate-buffered saline (PBS) and subcutaneously inoculated into the right scapular region of each mouse on day 0.

To assess *in vivo* mRNA delivery, 4T1 tumor-bearing mice (n = 3 on day 21) received a single peritumoral subcutaneous injection of PFHA-PEI-mRNA-HP loaded with luciferase mRNA (Luc mRNA) near the tumor site. At 4 h post-injection, the mice were administered luciferin substrate (6 mg for each mouse) *via* intraperitoneal injection and imaged using an IVIS spectrum *in vivo* imaging system to detect bioluminescence.

For therapeutic evaluation, the mice were randomly assigned to treatment groups (n = 5). On day 3, the mice received a 100 μL subcutaneous injection of PFHA-PEI-mRNA-HP loaded with IL12 mRNA (15 μg mRNA per mouse). On day 4, the mice were

administered 100 μL of anti-PD-L1 antibody (100 μg per mouse, dissolved in PBS) *via* subcutaneous injection. The control groups included an anti-PD-L1-only group (n = 3) and an untreated group (n = 3). Tumor growth was monitored using digital calipers, and tumor volume was calculated using the formula $V = 0.5x \times Lx \times W^2$, where L and W represent the length and width of the tumor, respectively. Tumor measurements were recorded every 2–3 days from day 3 to day 14. On day 14, the mice were euthanized, and the tumors were excised for analysis.

For biosafety evaluation, the mice (n = 3) received a 100 μL subcutaneous injection of PFHA-PEI-mRNA-HP loaded with EGFP mRNA (15 μg mRNA per mouse). The untreated mice (n = 3) were used as the control. The body weight of the mice was measured at day 0, day 1 and day 14. Blood samples were collected *via* submandibular puncture and subjected to blood chemistry analysis (Moichor, San Francisco, CA, USA) to evaluate key biochemical markers, including glucose (GLU), blood urea nitrogen (BUN), albumin (ALB), alanine aminotransferase (ALT), and aspartate aminotransferase (AST).

2.17 Statistical analysis

The results are presented as mean value ± standard error of the mean. The statistical differences were determined by two-sided unpaired Student's t-test in most of the analyses, except Fig. 9d, where one way ANOVA with Tukey's HSD *post hoc* test was applied. The values were considered statistically significant at $p < 0.05$. In the figure presentations, n.s. means statistically not significant, * means $p < 0.05$, ** means $p < 0.01$, and *** means $p < 0.001$.

3. Results and discussion

3.1 Design and synthesis of PFHA-PEI-mRNA-HP

The molecular properties such as molecular weight, polarity and functional groups of each of the constituents of PFHA-PEI-mRNA-HP were considered for selection. PFHA was chosen considering its appropriate chain length given that PFHA being too long would compromise the aqueous solubility of the mRNA complex, while too short would diminish its utility in the system. Branched PEI with a molecular weight of 2 kDa was selected owing to its relatively strong nucleic acid condensing capability and innocuous toxicity profiles. Given that high molecular weight heparin could compete with mRNA for electrostatic binding and cause large-size aggregation, HP was chosen due to its small size which is beneficial for controlling the size and integrity of the mRNA complex. PFHA was conjugated on PEI (branched, MW 2 kD) *via* EDC/NHS coupling chemistry (Fig. 1a). The PFHA : PEI molar ratio for coupling was set at 7 : 1 for conjugation, given that this ratio (*i.e.*, PFHA : PEI/7 : 1) yielded the best transfection results compared to other ratios (Fig. S1).

A rotor-syringe mixing (RSM) platform was set up by combining a microliter syringe-loaded syringe pump, a mechanical rotor equipped with a disposable stirring head and a lifting sample tube holder into a solution mixing system to assemble

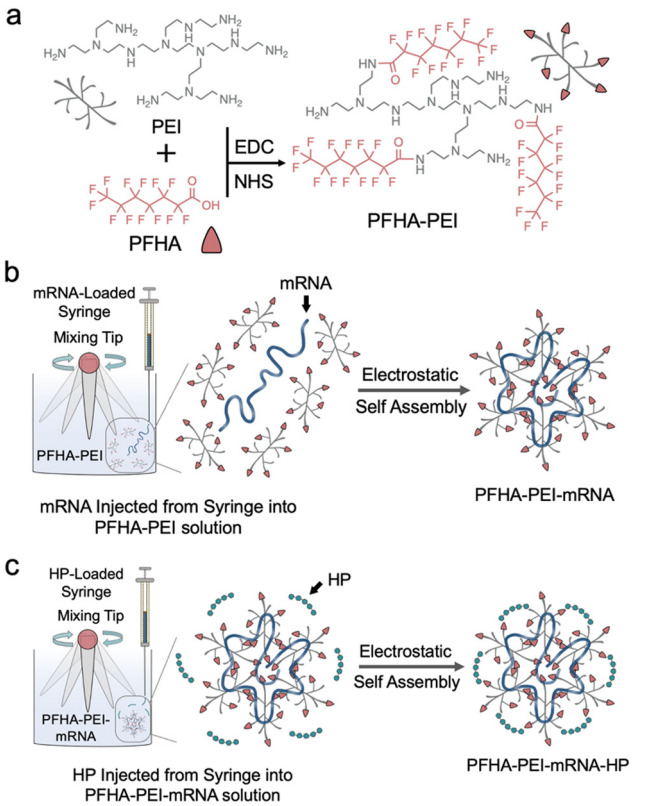

Fig. 1 Schematic of the synthesis of PFHA-PEI-mRNA-HP. (a) Reaction scheme for conjugating PFHA onto PEI *via* EDC/NHS coupling chemistry. For clarity, a monomeric PEI unit is shown rather than the full branched structure of 2 kDa PEI used in the synthesis. The schematic depicts conjugation to a primary amine, which is favored due to its higher nucleophilicity and accessibility. The PFHA : PEI ratio is not drawn to scale; the actual substitution was determined by ^{19}F NMR to be approximately 4.79 : 1 (see Fig. S5). (b) Illustration of the process of mRNA being condensed by PFHA-PEI. mRNA solution was loaded into a syringe and injected into the PFHA-PEI solution at a fixed flow rate (1 μL s^{-1}) while the solution was stirred by a rotor tip (500 rpm) for homogeneous mixing. (c) Illustration of the process of embellishing the surface of PFHA-PEI-mRNA with HP. HP solution was loaded into a syringe and injected into the PFHA-PEI-mRNA solution at a slow flow rate (0.5 μL s^{-1}) while the solution is stirred by a rotor tip (500 rpm) for homogeneous mixing.

PFHA-PEI, mRNA and HP into PFHA-PEI-mRNA-HP nanoparticles. With precise control over the stirring speed and injection flow rate, the RSM platform ensured consistent mixing efficiency and complexing outcomes when preparing the mRNA complex. The core of the nanoparticle is composed of mRNA condensed by PFHA-PEI to render structural compactness for mRNA protection. The PFHA-PEI-mRNA complex was first formed by slowly injecting mRNA solution at 1 μL s^{-1} into PFHA-PEI solution, which was being stirred at 500 RPM by the RSM platform (Fig. 1b). Injecting mRNA into PFHA-PEI solution instead of the other way around ensured that each mRNA molecule can be fully covered and condensed upon contact with PFHA-PEI. The PFHA-PEI : mRNA wt/wt ratio was set at 15 : 1 for optimal physicochemical properties and transfection compared to other ratios based on the screening results (Fig. S2).

Subsequently, the surface of the PFHA-PEI-mRNA core was decorated with HP to form an outer shell layer for tuning the binding tightness of mRNA in the core, and in turn facilitating the intracellular delivery of the mRNA payload. A pre-calculated amount of HP was injected into the PFHA-PEI-mRNA solution at 0.5 μL s^{-1} while it was being stirred at 500 RPM *via* the same RSM device to complete the formation of the PFHA-PEI-mRNA-HP nanoparticles. Given that injecting PFHA-PEI-mRNA directly into the HP solution would cause excessive binding of HP onto each PFHA-PEI-mRNA complex and result in overwhelming electrostatic binding competition between HP and mRNA, HP was injected into the PFHA-PEI-mRNA solution at a slow speed to achieve gradual HP surface embellishing on PFHA-PEI-mRNA (Fig. 1c).

3.2 Physicochemical property characterization

FTIR and XPS were performed on the purified PFHA-PEI product to confirm the presence of PFHA on PEI after conjugation. The purity of PFHA-PEI was evaluated by high-performance liquid chromatography (HPLC). The retention time of PFHA, PFHA-PEI and PEI was 18, 23 and 36 min, respectively (Fig. S3). The fact that the spectrum of PFHA-PEI did not contain noticeable peaks from pure PFHA and pure PEI suggests the high purity of PFHA-PEI. The FTIR analysis revealed the formation of an amide bond between PFHA and PEI, which was absent in the spectra of pure PFHA and PEI (Fig. 2a). The unique peak pattern of PFHA was also found by adding the peak pattern of PEI to the spectrum of PFHA-PEI, indicating the successful conjugation of PFHA on PEI. The XPS analysis (Fig. 2b) and

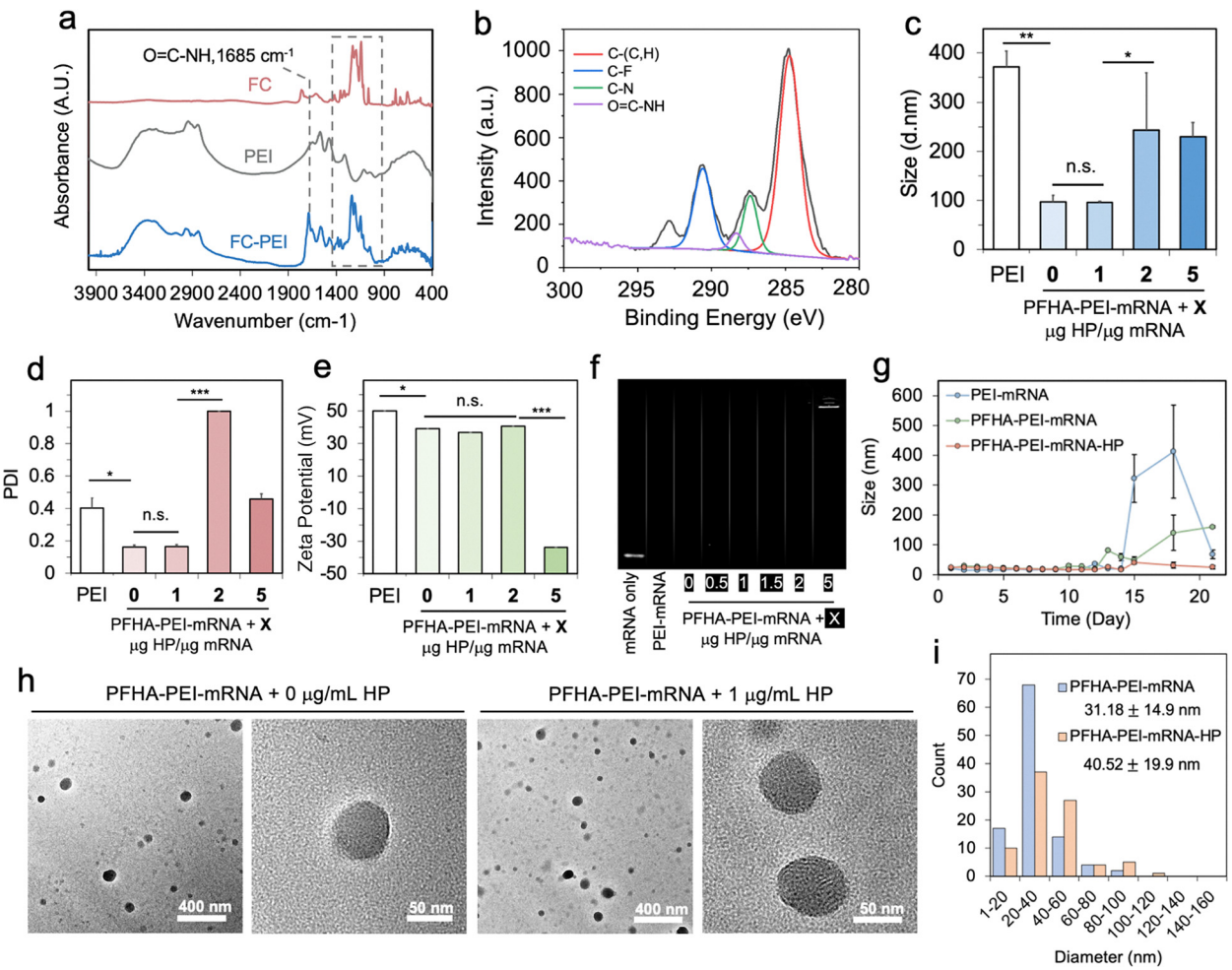

Fig. 2 Physicochemical characterization of PFHA-PEI-mRNA-HP. (a) FTIR spectra of PFHA, PEI and PFHA-PEI. The gray dashed box marks the region of the addition of characteristic peak patterns from the spectrum of PFHA to the spectrum of PEI. The gray dashed line indicates the presence of amide bonds between PFHA and PEI. (b) X ray photoelectron spectroscopy (XPS) spectrum of PFHA-PEI with peak fitting analysis. Hydrodynamic size (c), polydispersity index (d) and zeta potential (e) measurements of PEI-mRNA, PFHA-PEI-mRNA and PFHA-PEI-mRNA-HP with various HP amounts. For the labels on the *x* axis of (c)–(e), PEI represents PEI-mRNA. 0, 1, 2, and 5 correspond to PFHA-PEI-mRNA + 0, 1, 2, and 5 μg HP per μg mRNA, respectively. (f) Gel retardation assay of PEI-mRNA, PFHA-PEI-mRNA and PFHA-PEI-mRNA-HP (with different HP amounts) with free mRNA as the control. (g) Serum stability data of PEI-mRNA, PFHA-PEI-mRNA and PFHA-PEI-mRNA-HP with mRNA : HP ratio of 1 : 1 wt/wt All samples were placed in PBS supplemented with 10% v/v FBS solutions and incubated at 37 °C. (h) TEM images of PFHA-PEI-mRNA-HP (with different HP amounts) at high and low magnifications. The scale bars are 400 nm and 50 nm, respectively. (i) Size distribution profiles of PFHA-PEI-mRNA (no HP) and PFHA-PEI-mRNA-HP NPs from the low-magnification TEM images in (h).

Raman spectroscopy analysis (Fig. S4) of PFHA-PEI also confirmed the presence of an amide bond between PFHA and PEI. The fluorination degree of PEI was characterized by quantitative ^{19}F NMR. Employing trifluoroacetic acid (TFA), with its characteristic $-CF_3$ peak at -76.15 ppm, as the internal standard, the unique $-CF_3$ triplet peaks of PFHA on PFHA-PEI at around -82.4 ppm was used to calculate the fluorination degree of PEI.[44] The quantitative results by comparing the integrated area under peaks of $-CF_3$ from PFHA to that from TFA revealed that the PFHA : PEI molar ratio in PFHA-PEI was 4.79 : 1 (Fig. S5). These results collaboratively validated the successful synthesis of PFHA-PEI.

Size, surface charge and shape all play critical roles in determining the cellular uptake amount, intracellular fate, and eventual success of payload delivery of nanoparticles. Spherical, cationic nanoparticles with a diameter of 30–150 nm have been shown to have balanced performance in blood/serum stability, cellular uptake amount and endosomal escape efficiency.[45] Hence, the hydrodynamic size and surface charge of the PFHA-PEI-mRNA-HP nanoparticles were measured to study their suitability for intracellular mRNA delivery. The influence of each component of the PFHA-PEI-mRNA-HP nanoparticle on its overall hydrodynamic size and surface charge was investigated. Without PFHA and HP, branched PEI with a molecular weight of 2 kDa alone could effectively condense mRNA into a compact nanoparticle given that PEI-mRNA has a diameter larger than 350 nm and a high polydispersity index of >0.4 (Fig. 2c and d), respectively. When PFHA was integrated into the system, PFHA-PEI could condense mRNA into a nanoparticle smaller than 100 nm in size with PDI of <0.2. The further incorporation of HP (mRNA : HP wt/wt ratio of 1 : 1) did not increase the size and PDI of the PFHA-PEI-mRNA nanoparticles, indicating that adding HP at this amount neither affected the compactness nor the uniformity of the PFHA-PEI-mRNA nanoparticles. The zeta potential measurements yielded a value close to 40 mV for the PFHA-PEI-mRNA and PFHA-PEI-mRNA-HP nanoparticles, and a value close to 50 mV for PEI-mRNA (Fig. 2e). It is reasonable that PEI-mRNA would possess a slightly higher surface charge due to its much larger size than the other two nanoparticle formulations, and hence would carry more positive charges. Although PFHA-PEI-mRNA is much smaller than PEI-mRNA, its zeta potential (between 35 and 40 mV) is only slightly lower than that of PEI-mRNA. This phenomenon suggests that PFHA-PEI-mRNA possesses a higher charge density than PEI-mRNA. Since structural compactness is challenging to maintain at a high charge density due to the repulsion between the same charges, additional favorable energy is required to overcome the structurally destabilizing electrostatic repulsion. The addition of a single component, PFHA, helped maintain the compactness of the PEI-mRNA complex, indicating that the tendency of PFHA to self-assemble could be the driving energy to overcome the same charge repulsion in this system. The relatively high surface charge of PFHA-PEI-mRNA may limit its suitability for systemic (*e.g.*, intravenous) administration due to its potential rapid clearance by the mononuclear phagocyte system and increased serum protein adsorption. Thus, future studies should explore surface modification strategies, such as PEGylation and use of charge-shielding polymers, to improve its systemic circulation properties if intravenous delivery is pursued.

Since heparin is a polyanion that could compete with mRNA for electrostatic binding and induce the formation of large aggregates between cationic complexes due to charge neutralization, it is crucial to tune the amount of HP in mRNA complexes. When added at the desired amount without affecting the overall stability of mRNA complexes, HP could partially shield the positive charges on cationic mRNA complexes to increase their biocompatibility and alleviate the binding tension between mRNA and cationic polymers to facilitate the release of mRNA for translation in the cytoplasm. Nevertheless, excess HP can result in the destabilization of the mRNA complex, and possibly premature mRNA release. Therefore, different amounts of HP were added to PFHA-PEI-mRNA to create different versions of mRNA complexes to study the upper limit of HP at which the PFHA-PEI-mRNA-HP complex would disintegrate. At or below 1 : 1 wt/wt of mRNA : HP, the results suggest that PFHA-PEI-mRNA-HP retained a similar compact size and zeta potential to that of PFHA-PEI-mRNA (Fig. 2c, d and Fig. S6). Its size started to increase slightly at 1 : 1.5 wt/wt of mRNA : HP, indicating slight destabilization in the compactness of PFHA-PEI-mRNA. At 1 : 2 wt/wt of mRNA : HP, the size of PFHA-PEI-mRNA-HP drastically increased from sub-hundred nm to >240 nm and its PDI was close to 1, indicating the formation of highly polydisperse and aggregated NPs (Fig. 2c and d), respectively. Even though the zeta potential of PFHA-PEI-mRNA-HP at 1 : 2 wt/wt of mRNA : HP remained at 40 mV, its much larger hydrodynamic size indicates that the charge density was significantly lower than that of the nanoparticles prepared using 1 : 1 wt/wt of mRNA : HP. This data indicates that HP started to destabilize PFHA-PEI-mRNA at mRNA : HP of 1 : 2 wt/wt and caused the formation of large aggregates. However, mRNA remained largely unexposed given that its zeta potential remained at a highly positive value. With a further increase in the amount HP to mRNA : HP of 1 : 5 wt/wt, the zeta potential of PFHA-PEI-mRNA-HP completely reverted to a negative value, suggesting the release of the large anionic mRNA molecules and full disintegration of PFHA-PEI-mRNA-HP. The hydrodynamic and zeta potential results were corroborated by a gel retardation assay. According to the gel image (Fig. 2f), there were noticeable mRNA signals from the wells of PFHA-PEI-mRNA-HP at 1 : 5 wt/wt of mRNA : HP, which can be attributed to the partial exposure of the released mRNA from this sample. Meanwhile, there was no detectable signal in the wells loaded with PFHA-PEI-mRNA at other mRNA : HP ratios, suggesting that mRNA was well protected and unexposed in these samples. The transfection test with various HP amounts demonstrated that the optimal transfection results were obtained with a 1 : 1 wt/wt ratio of mRNA : HP on 2 different cell lines (Fig. S7). Based on these results, PFHA-PEI-mRNA with 1 : 1 wt/wt of mRNA : HP can fully condense mRNA and is optimal in terms of size, zeta potential and transfection efficiency.

The mRNA encapsulation study was conducted with free mRNA as the positive control and PFHA-PEI-HP (HP amount equivalent to that of mRNA : HP wt/wt ratio of 1 : 1) as the

mRNA-free negative control. PFHA-PEI-mRNA-HP with the mRNA : HP ratio of 1 : 1 wt/wt was selected as the testing groups. The encapsulation results suggest that PFHA-PEI-mRNA-HP with the mRNA : HP ratio of 1 : 1 wt/wt could achieve an mRNA encapsulation efficiency of 89%, which is comparable to other similar highly efficient mRNA delivery vehicles (Fig. S8).[46,47] Moreover, PFHA-PEI-mRNA-HP with an mRNA : HP ratio of 1 : 1 wt/wt exhibited superior serum stability to PEI-mRNA and PFHA-PEI-mRNA (Fig. 2g). PFHA-PEI-mRNA-HP was able to consistently retain its small size in the serum-supplemented solution for over 21 days, while PFHA-PEI-mRNA and PEI-mRNA showed unstable size fluctuation starting after day 13. This could be attributed to the contribution of HP in shielding PFHA-PEI-mRNA-HP from excessive serum protein adsorption to prevent the formation of large aggregates. The fact that PEI-mRNA showed a much larger size fluctuation than PFHA-PEI-mRNA suggests that PFHA also contributed to the serum stability of the mRNA complex in this case.

TEM imaging was performed to provide visual confirmation of the compact sizes of PFHA-PEI-mRNA and PFHA-PEI-mRNA-HP. PFHA-PEI-mRNA exhibited a relatively uniform size and spherical shape profile, as evidenced in both its high- and low-magnification TEM images (Fig. 2h). Upon the addition of 1 μg mL^{-1} HP, PFHA-PEI-mRNA-HP exhibited similar size and shape profiles to PFHA-PEI-mRNA. The particle size analysis on the low-magnification TEM images revealed that the average dry diameters of PFHA-PEI-mRNA and PFHA-PEI-mRNA-HP were 31.18 nm and 40.52 nm, respectively (Fig. 2i). These observations suggest that the incorporation of HP at this concentration did not destabilize PFHA-PEI-mRNA, indicating the preservation of its original properties. The hydrodynamic size measurement data further supported this finding. However, it was noted that the destabilization of these nanoparticles could occur at higher HP concentrations, potentially attributing to the binding competition between the anionic HP and mRNA. The TEM imaging results corroborated these observations. Starting with just the PEI-mRNA complex, the resultant structure was hundreds of nm in size with amorphous shapes (Fig. S9). The introduction of PFHA led to the formation of a compact spherical nanostructure. This notable transformation in structure could be attributed to the spontaneous self-assembly of PFHA, as described before. Drastic structural changes in PFHA-PEI-mRNA-HP were observed when the mRNA : HP ratio was further increased to 1 : 2 wt/wt, and eventually 1 : 5 wt/wt At 1 : 2 wt/wt of mRNA : HP, aggregates with sizes much larger than 200 nm and irregular shape were observed (Fig. S9). At 1 : 5 wt/wt of mRNA : HP, clear disintegration of PFHA-PEI-mRNA-HP was observed. These imaging results agree with the previous hydrodynamic size and zeta potential results, as they all reveal the critical instability point of PFHA-PEI-mRNA-HP at 1 : 2 wt/wt of mRNA : HP and full disintegration at 1 : 5 wt/wt of mRNA : HP. Combined with its high mRNA loading efficiency and serum stability, PFHA-PEI-mRNA-HP with the mRNA : HP wt/wt ratio of 1 : 1 was selected as the optimal formulation for the downstream studies.

3.3 Cellular uptake and endosomal escape

As an essential step toward the downstream transfection success, the cell uptake and endosomal escape performance of the PFHA-PEI-mRNA-HP nanoparticles must be evaluated. As a fragile biomolecule prone to degrade, mRNA needs to be protected from RNases during its transportation to the cell surface, effectively ferried across the cell plasma membrane, escape from endo-lysosomes to avoid digestion, and eventually released into the cytoplasm for translation. Although PFHA-PEI-mRNA-HP shows promising physicochemical properties, its cellular interactions are still largely unknown because the interaction of nanoparticle with cells in biological medium is far too complex for mere size, shape, and surface charge profiles to dictate. The avoidance of trapping in digestive lysosomal compartments can be a hallmark of a highly efficient transfection agent such as Lipofectamine.[48] Therefore, understanding the cell uptake and the endosomal escape performance is essential for developing successful transfection agents.

4T1 and M6 mouse breast cancer cells were chosen due to their capability to form syngeneic mouse tumors that closely mimic human metastatic breast tumors.[49,50] In addition, the HepG2 human liver cancer cell line was also chosen as it is extensively studied for oncogenesis and drug screening purposes.[51] PFHA-PEI-mRNA-HP with mRNA tagged with Cy5 fluorophores was incubated with 4T1, M6 and HepG2 cancer cells at 37 °C for 12 h. LysoTracker was added to the cell culture 1 h before the incubation period ended. Z-Stacked fluorescent images were utilized, and subsequently 3D-rendered into a surface-and-spots model to illustrate the precise locations of the cell nuclei, mRNA and endo-lysosomes (Fig. 3a). In these imaging results, the Cy5 signal emitted from PFHA-PEI-mRNA-HP exhibited distinct spatial separation from the LysoTracker signal across all three cell lines. This observation suggests that the majority of PFHA-PEI-mRNA-HP did not become trapped in the digestive lysosome.

Cross-sectional views of the 3D images, taken from sagittal, coronal and transverse planes, confirmed the separation between PFHA-PEI-mRNA-HP and the LysoTracker signals (Fig. 3b). A top-down view of the 3D-rendered model was also generated to better reveal the separation between the mRNA Cy5 signal and the LysoTracker signal, offering an unobstructed perspective (Fig. 3c). The 3D colocalization analysis revealed that the volumetric Pearson coefficient between the mRNA and the LysoTracker signals was consistently below 0.2 across all three cell lines tested, suggesting that the majority of the mRNA delivered by PFHA-PEI-mRNA-HP successfully escaped from lysosome entrapment, regardless of the cell type (Fig. 3c).[52,53]

To investigate the contribution of each component of PFHA-PEI-mRNA-HP to cellular uptake and endosomal escape, PEI-mRNA and PFHA-PEI-mRNA were also loaded with Cy5-tagged mRNA and incubated with all three cell lines for comparative analysis. The images revealed that the cells treated with PEI-mRNA exhibited insufficient or negligible cellular uptake, potentially due to the large size of PEI-mRNA and its limited

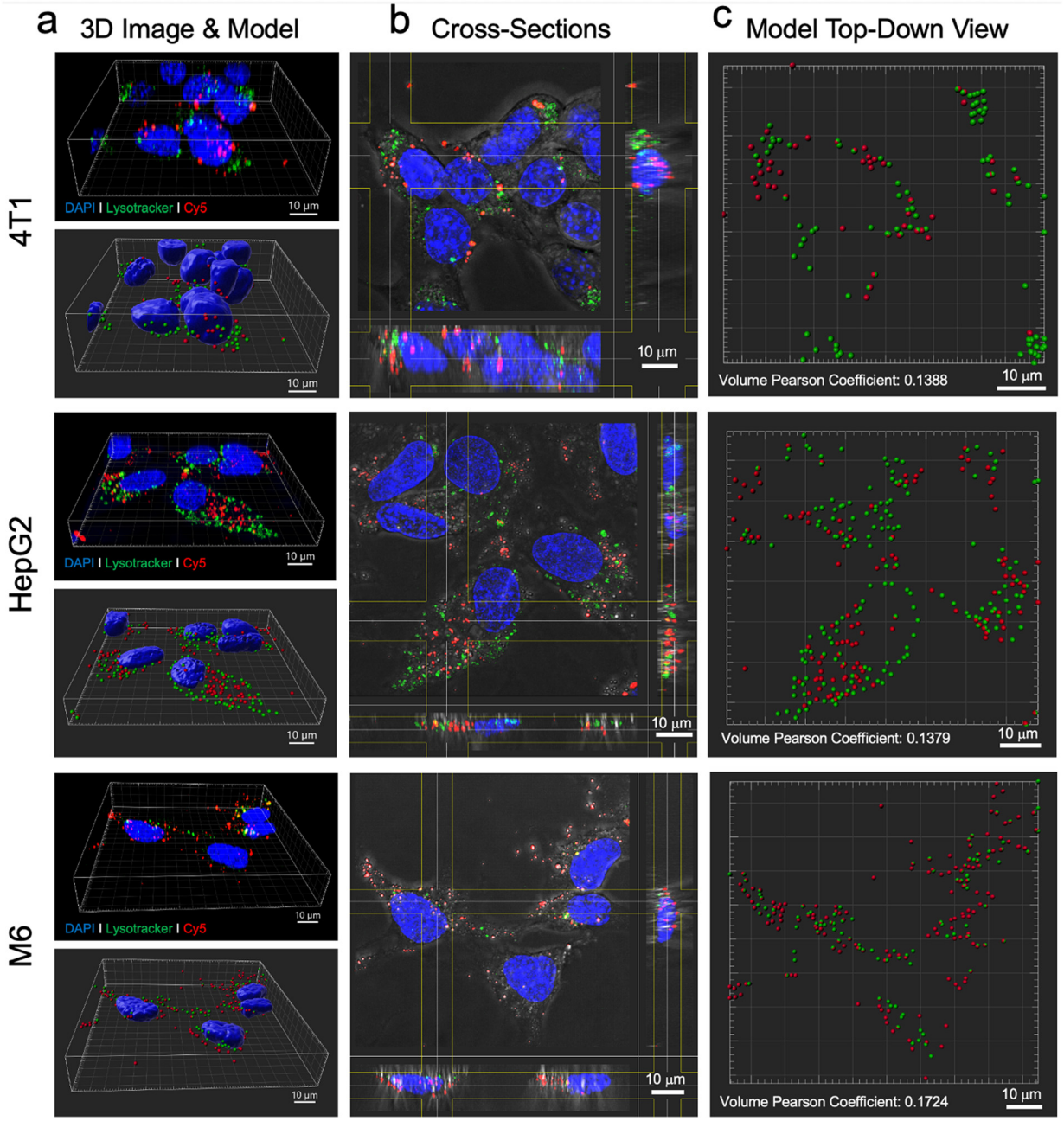

Fig. 3 Cell uptake and endosomal escape studies of PFHA-PEI-mRNA-HP on 3 different cancer cell types. All treatments were applied to cells at 37 °C for 12 h at an mRNA concentration of 2 μg mL^{-1} and 3D Z stacked confocal images were taken with a z-resolution of 0.5 μm. The blue color represents cell nuclei; green represents LysoTracker and red represents mRNA. (a) Z-stacked 3D images (top panel) and 3D-rendered models (bottom panel) of three cancer cell lines treated with PFHA-PEI-mRNA-HP. In the 3D rendered models, cell nuclei are presented as blue surface, and green and red spots represent endo-lysosomes and mRNA, respectively. (b) Cross-sectional images of the z-stacked 3D images in (a) viewing from coronal, sagittal and transverse planes with bright field image as the background. (c) Top-down view of the 3D-rendered model (a) excluding cell nuclei. 3D viewing, model rendering and colocalization analysis were performed on the IMARIS image analysis software (Oxford Instruments).

ability to penetrate the plasma membrane (Fig. S10). Nonetheless, for the minority of PEI-mRNA particles that managed enter the cytoplasm, they demonstrated effective avoidance of colocalization with endolysosomes, which is likely due to the intrinsic capability of PEI to overcome endosomal entrapment.[54]

On the other hand, PFHA-PEI-mRNA demonstrated markedly higher cellular uptake across all 3 cell lines compared to PEI-mRNA. This enhanced uptake can be attributed to the inherent tendency of PFHA to self-assemble and its biphasic separation property in both aqueous and organic phases. The compact nature of PFHA-PEI-mRNA allows it to easily traverse the lipid-water interface, resulting in a substantial increase in its cellular uptake. The unique combination of the ability of PFHA for biological membrane penetration and capability of

PEI for endosomal escape contributes to the sustained efficiency of PEHA-PEI in evading endosomal entrapment. The introduction of HP further enhances its cellular uptake, while retaining the rapid endosomal escape characteristic of PFHA-PEI-mRNA. The enhanced intracellular nanoparticle accumulation observed with the addition of heparin is likely due to the improved serum stability, as heparin may partially shield the positive surface charge of the polyplex and reduce its non-specific adsorption to serum proteins, thereby minimizing its premature clearance and allowing more nanoparticles to reach and enter the target cells. Another possibility of this higher cell uptake is that HP might slightly loosen the binding of PFHA-PEI to mRNA, exposing the mRNA more prominently for fluorescent detection. In summary, each component of PFHA-PEI-mRNA-HP plays a crucial role in its cellular uptake and endosomal escape. PEI contributes endosomal escape capability, PFHA provides efficient biological membrane penetration, and HP enhances the cell uptake and mRNA release.

Confocal microscopy images taken at an earlier time point (3 h post-treatment) for PFHA-PEI-mRNA-HP on 4T1 and HepG2 cells at an mRNA concentration of 2 μg mL^{-1} provided further insights into its cellular uptake and endosomal escape dynamics (Fig. S11). These images show that many nanoparticles are attached to the cell membrane, and partial colocalization with endo-lysosomal compartments can occasionally be observed, particularly in the PFHA-PEI-mRNA-HP group.

A spherical nanoparticle with sub-hundred nm diameter and cationic surface charge typically enters cells *via* energy-dependent endocytosis. Since PFHA-PEI-mRNA-HP is a cationic spherical nanoparticle with sub-hundred nm diameter, and simultaneously possesses a hydrophobic moiety, PFHA, and cell receptor ligand, HP, it is expected that PFHA-PEI-mRNA-HP would enter cells *via* the receptor-mediated energy-dependent endocytosis pathway. As energy-dependent pathways in cells are greatly inhibited at 4 °C,[55] the internalization of PFHA-PEI-mRNA-HP should be mostly halted at this temperature if endocytosis is responsible for cell uptake in this case. A cellular uptake study where PFHA-PEI-mRNA-HP was applied to all three cell lines and incubated at 4 °C was conducted in parallel to the experiments conducted at 37 °C to validate this view. Compared to the PFHA-PEI-mRNA-HP nanoparticles that were internalized into deep intracellular space when incubated with cells at 37 °C, the imaging results from all 3 cell lines treated at 4 °C unanimously show that the PFHA-PEI-mRNA-HP nanoparticles were either anchored on the surface of the plasma membrane without internalization or only achieved shallow penetration into the cytoplasm (Fig. S12). Notably, the evident LysoTracker signal presented in the cells incubated at 37 °C mostly disappeared in the cells incubated at 4 °C. The fact that the LysoTracker signal was barely observable in the cells incubated at 4 °C could be an indicator of greatly suppressed endocytosis at this low temperature. These results collectively pointed out that even though PFHA-PEI-mRNA-HP could still bind to the cell plasma membrane *via* electrostatic adsorption at a lower temperature, it could not be efficiently internalized with endocytosis being effectively halted at 4 °C. Therefore, the energy-dependent endocytosis is primarily responsible for the cellular internalization of PFHA-PEI-mRNA-HP.

3.4 Biocompatibility tests

PEI-mRNA, PFHA-PEI-mRNA, PFHA-PEI-mRNA-HP and Lipofectamine 2000-mRNA were applied to the 4T1, HepG2 and M6 cell lines to assess their biocompatibility based on the quantitative Alamar blue cell viability assay results and observations from bright field cell images. The 4T1 cells treated with PFHA-PEI-mRNA-HP were able to retain around 90% viability across the mRNA concentration ranging from 0 to 3 μg mL^{-1} (Fig. 4a). On the other hand, Lipofectamine 2000-mRNA inflicted more than 20% viability loss on 4T1 at 2 μg mL^{-1} and above. The toxicity inflicted by PFHA-PEI-mRNA falls between that by PFHA-PEI-mRNA-HP and Lipofectamine 2000-mRNA, while PEI-mRNA exerted the highest toxicity on 4T1 by reducing its viability to around 70% at 2 μg mL^{-1} and above. On the HepG2 cell line, Lipofectamine 2000-mRNA exhibited a clear trend in its toxicity profile. As the mRNA concentration increased from 0 to 3 μg mL^{-1}, the viability of the HepG2 cells decreased from 100% to around 70%, and eventually 60% (Fig. 4a). The PEI-mRNA-treated

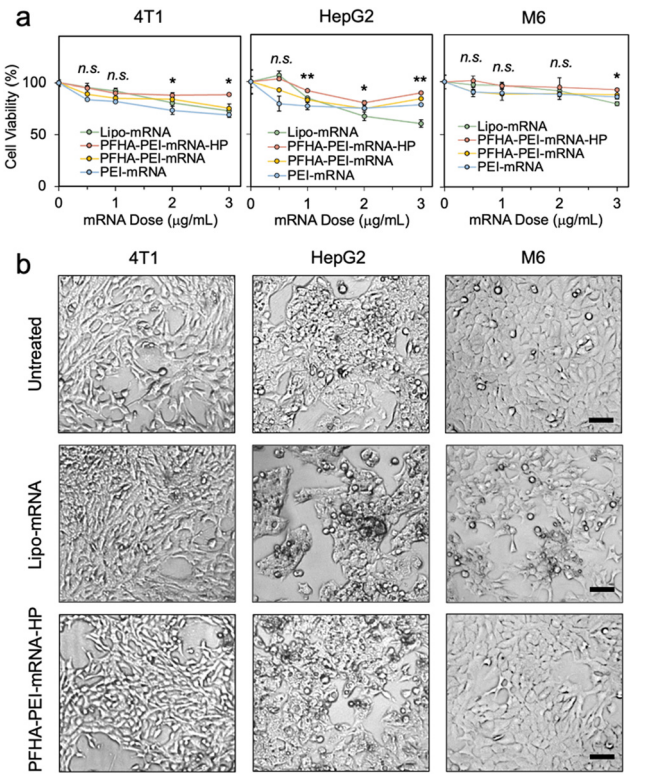

Fig. 4 Cell viability test results of PFHA-PEI-mRNA-HP. (a) Quantitative Alamar Blue cell viability assay results on 4T1, HepG2 and M6 cells. Each cell type was treated with PEI-mRNA, PFHA-PEI-mRNA, PFHA-PEI-mRNA-HP and Lipofectamine 2000-mRNA at 0, 5, 1, 2 and 3 μg mL^{-1} for 24 h. The untreated cell viability was normalized to 100% for all cell lines. Statistical analysis was performed to determine if the difference between the data points from the Lipo-mRNA-treated cells and the data points from other treated cells was significant. (b) Representative bright field images of untreated, Lipofectamine 2000-mRNA-treated and PFHA-PEI-mRNA-HP-treated cells at 2 μg mL^{-1} mRNA concentration. Scale bar is 50 μm.

HepG2 cells consistently showed around 75% viability at an mRNA concentration between 0.5 to 3 μg mL^{-1}. On the other hand, the PFHA-PEI-mRNA or PFHA-PEI-mRNA-HP-treated HepG2 cells were mostly able to retain >80% viability in the mRNA concentration range of 0.5 to 3 μg mL^{-1}. On the M6 cell line, the cells treated with PFHA-PEI-mRNA exhibited a remarkable retention of viability higher than 90% at a 3 μg mL^{-1} dose. In comparison, the cells treated with PEI-mRNA and PFHA-PEI-mRNA retained ~85% viability. Notably, the cells treated with Lipofectamine 2000-mRNA experienced a more significant decline, dropping below 80% viability at the same 3 μg mL^{-1} mRNA dose.

The quantitative cell viability assay results were corroborated by the bright field images. The bright field images of the untreated or the PFHA-PEI-mRNA-HP-treated 4T1 cells showed a similar cell density and morphology, which suggests that the proliferation rate and health of the 4T1 cells were not significantly affected by the presence of PFHA-PEI-mRNA-HP (Fig. 4b). The 4T1 cells treated with PEI-mRNA, PFHA-PEI-mRNA and Lipofectamine 2000-mRNA showed a slightly lower cell density than the untreated cells, agreeing with 4T1 cell viability results that these treatments inflicted mild toxicity on the 4T1 cells (Fig. 4b and Fig. S13). Although the PFHA-PEI-mRNA-HP-treated HepG2 cells displayed a similar cell density as the untreated cells, the morphology of the treated HepG2 cells appeared to be slightly clumpier and more corrugated than the untreated cells (Fig. 4b). This corresponds to the slight decrease in the viability of the HepG2 cells treated by PFHA-PEI-mRNA-HP at 2 μg mL^{-1} mRNA. The HepG2 cell images also confirmed that Lipofectamine 2000-mRNA indeed caused noticeable cytotoxicity to the HepG2 cells as their cell density was significantly lower and their cell morphology appeared to be clumpier. Meanwhile, PEI-mRNA and PFHA-PEI-mRNA only displayed mild adverse effects on the HepG2 cells, as the cell viability results suggested (Fig. S13). The bright field images of M6 cells did not show noticeable differences in terms of cell density and morphology between the PFHA-PEI-mRNA-HP-treated, PFHA-PEI-mRNA-treated and the untreated cells, which agrees well with the cell viability test results (Fig. 4b and Fig. S13). One the other hand, the M6 cells treated with PEI-mRNA and Lipofectamine 2000-mRNA exhibited lower confluency, along with notable cell shrinkage and clustering. These observations collectively suggest the poorer biocompatibility associated with these two treatments. To validate that the cells visualized in the bright field images were indeed viable, live/dead staining was performed using Calcein AM and propidium iodide (Fig. S14). The results confirmed that the majority of cells under each treatment condition were alive, further supporting the conclusion that PFHA-PEI-mRNA-HP exhibits minimal cytotoxicity across all the tested cell lines.

Taking all the biocompatibility data together, both PFHA-PEI-mRNA-HP and PFHA-PEI-mRNA displayed reliable biocompatibility across all 3 cell lines because they typically inflict less than 20% growth retardation even at an mRNA concentration as high as 3 μg mL^{-1}. The fact that the PFHA-PEI-mRNA-HP-treated cells consistently showed slightly higher viability than that treated by PFHA-PEI-mRNA could suggest the contribution of HP to improving the biocompatibility of the mRNA complex. Without PFHA and HP, the toxicity of PEI-mRNA could be obvious on some cell lines. These results indicate that HP and PFHA are both beneficial in alleviating the toxicity from PEI. Although Lipofectamine 2000-mRNA showed decent biocompatibility on 4T1 cells, it inflicted noticeable toxicity on HepG2 and M6 cells at elevated mRNA concentrations, and thus it can pose safety concerns when applied to certain cell types. Importantly, PFHA-PEI-mRNA-HP also showed promising results in the biocompatibility test in mice, suggesting that PFHA-PEI-mRNA-HP could be safe for future *in vivo* applications.

3.5 Transfection efficiency of multiple cell lines

PEI-mRNA, PFHA-PEI-mRNA, and PFHA-PEI-mRNA-HP nanoparticles were applied to the 4T1, HepG2 and M6 cell lines to test how each component of PFHA-PEI-mRNA-HP could affect transfection outcomes. The mRNA dosages needed to achieve the optimal transfection efficiency on different cell types were determined by a dose sensitivity study (Fig. S15). Through the dose sensitivity study, the mRNA concentration for transfecting all cancer cells was set at 2 μg mL^{-1}. As the ''gold standard'' of commercially available transfection agents touting high transfection efficiency and safety, Lipofectamine 2000-mRNA LNP was used as a positive control for comparison.[48] Based on the fluorescent image results (Fig. 5a and b), the incorporation of PFHA into PEI-mRNA significantly boosted the mRNA transfection efficiency in all cell lines. The conspicuous improvement in transfection could be attributed to the inertness, hydrophobicity as well as lipophobicity of PFHA. Since it is unfavorable for PFHA to interact with either a polar or non-polar environment, PFHA can self-assemble into compact structures with itself and remain inert to its environment. These characteristics render PFHA ideal for protecting fragile payloads such as easily degraded mRNA. The addition of HP to PFHA-PEI-mRNA further significantly enhanced the transfection efficiency in all the cell lines. As observed in the previous intracellular trafficking results, the presence of HP significantly increased the cellular uptake of PFHA-PEI-mRNA-HP compared to its counterpart without HP, corroborating the enhancement effect of HP on transfection. As observed in the intracellular trafficking results, the addition of HP significantly enhanced the cellular uptake of PFHA-PEI-mRNA-HP compared to its HP-free counterpart, confirming the role of HP in boosting the transfection efficiency. This improvement may be attributed to multiple factors, including the increased serum stability due to partial shielding of the positive surface charge of the polyplex by heparin, which reduces its nonspecific adsorption to serum proteins and nanoparticle loss during incubation.

Additionally, previous studies suggest that heparin may bind to fibroblast growth factor receptors (FGFRs), which are often overexpressed in various cancers, potentially facilitating receptor-mediated uptake.[56–58] To investigate this possibility, we performed an FGFR inhibition study using the FGFR inhibitor PD173074. Cells were pretreated with the inhibitor prior to transfection with PFHA-PEI-mRNA-HP nanoparticles

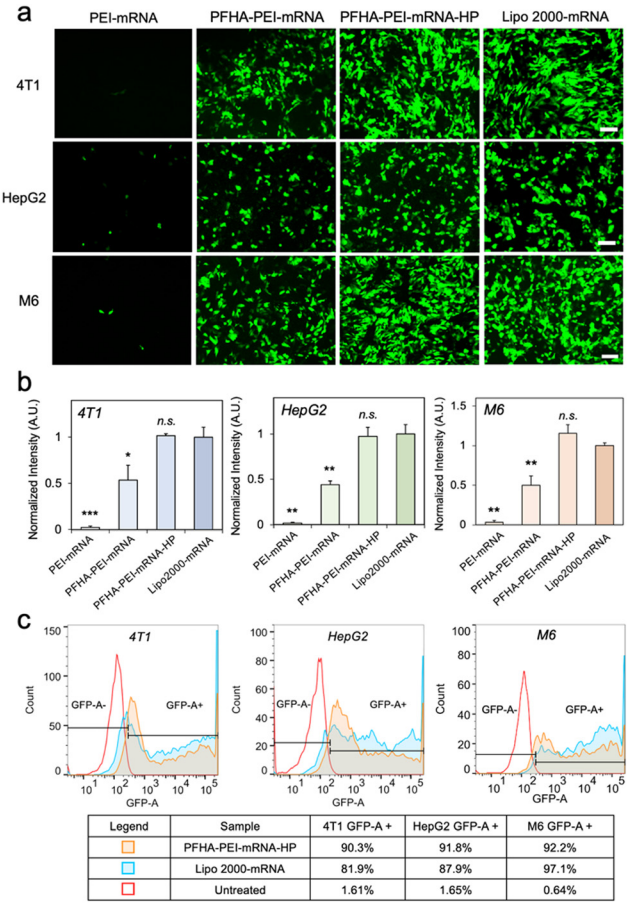

Legend	Sample	4T1 GFP-A +	HepG2 GFP-A +	M6 GFP-A +
	PFHA-PEI-mRNA-HP	90.3%	91.8%	92.2%
	Lipo 2000-mRNA	81.9%	87.9%	97.1%
	Untreated	1.61%	1.65%	0.64%

Fig. 5 Transfection results on three different cancer cell lines. (a) Transfection images of PEI-mRNA, PFHA-PEI-mRNA and PFHA-PEI-mRNA-HP, with Lipofectamine 2000-mRNA as the positive control on 4T1, HepG2 and M6 cells. Scale bar is 100 μm. (b) Quantitative analysis of the transfection results presented in (a). Statistical analysis was performed by comparing each treatment groups to the positive control Lipo2000-mRNA group. (c) Flow cytometric quantitative analysis of the transfection efficiency of PFHA-PEI-mRNA-HP with Lipofectamine 2000-mRNA as the positive control on three cancer cell lines.

(Fig. S16). No significant differences in EGFP expression were observed between the FGFR-blocked and unblocked groups in the 4T1, HepG2, and M6 cell lines. These results indicate that FGFR is not the primary mediator of cellular uptake in this system. Therefore, the HP-mediated enhancement of delivery is more likely attributed to physicochemical effects such as colloidal stability and charge modulation, rather than specific FGFR interactions.

The mechanism by which heparin enhances transfection may also be attributed to its ability to modulate the electrostatic interactions between the polymer and mRNA, facilitating a subtle packing–unpacking balance that promotes mRNA release in the cytoplasm, while still providing sufficient protection during cellular uptake and transport. However, the exact mechanism remains unclear and requires further investigation as an important direction for future research.

The transfection images show that PFHA-PEI-mRNA-HP was able to achieve comparable transfection efficiency to that of Lipofectamine 2000-mRNA on the 4T1, HepG2 and M6 cell lines. These image data combined with the physicochemical profiles of PFHA-PEI-mRNA-HP collectively showcase the importance of well-rounded attributes in size, shape, surface charge, biocompatibility, and intracellular trafficking profiles in successful mRNA transfection. Quantitative flow cytometric analysis was performed to study the percentage of successful transfected cell population from each cancer cell line (Fig. 5c). Similarly, the transfection performance of PFHA-PEI-mRNA-HP was compared to Lipofectamine 2000-mRNA in this study. The flow cytometry results showed that PFHA-PEI-mRNA-HP was able to achieve 90.3% and 91.8% transfection efficiency compared to slightly lower 81.9% and 87.9% by Lipofectamine 2000-mRNA on the 4T1 and HepG2 cell lines respectively. Meanwhile, PFHA-PEI-mRNA-HP was also able to transfect 92.2% of the M6 cell population, which was slightly lower than that of Lipofectamine 2000-mRNA of 97.1%.

To further validate the broad applicability of PFHA-PEI-mRNA-HP across different cancer types, three additional cell lines, human breast cancer (MCF7), human brain cancer (SF763), and rat brain cancer (C6), were subjected to transfection. These cell lines have been extensively utilized in cancer research.[59–61] Consistent with the transfection results observed in the 4T1, HepG2 and M6 cells, the addition of PFHA and HP to PEI-mRNA significantly enhanced the transfection efficiency on the MCF7, SF763 and C6 cells (Fig. 6a and b). The flow cytometry analysis showed that PFHA-PEI-mRNA-HP reliably achieved a high transfection efficiency of 90.3%, 83.9% and 85.8% compared to that of Lipofectamine 2000-mRNA of 71.6%, 87.2% and 79.1% on MCF7, SF763 and C6 cells, respectively (Fig. 6c). These transfection results collectively demonstrated that PFHA-PEI-mRNA-HP is highly effective in delivering mRNA to various cancer cell types. Moreover, it exhibited a similar or even superior performance when compared to the exemplary commercial LNP transfection platform, Lipofectamine, across several cell types. These findings position PFHA-PEI-mRNA-HP as a promising polymeric nano-construct candidate for achieving highly efficient mRNA transfection.

3.6 Stability of transfection efficiency after storage at 4 °C

The labile nature of mRNA poses significant challenges for its storage as it is highly susceptible to nucleases, oxidation, and hydrolysis.[62] The common storage conditions for mRNA complexes such as the COVID-19 mRNA vaccines developed by Pfizer-BioNTech and Moderna usually require deep-freezing at −80 °C or −20 °C. These vaccines not only are costly to distribute in cold-chain transportation but also only have a narrow window to be administered once thawed, which is usually within hours because frequent freeze–thaw cycle could easily jeopardize the structural integrity of mRNA.[3] Thus, the stable storage of mRNA complexes above 0 °C without freezing would greatly enhance their usability and transport. Even though lyophilization has been reported to significantly improve the stability of mRNA complexes above 0 °C,[63] the additional cost and labor for lyophilization and reconstitution later plus the quality control between these steps may bring more challenges and uncertainties for large-scale processing.

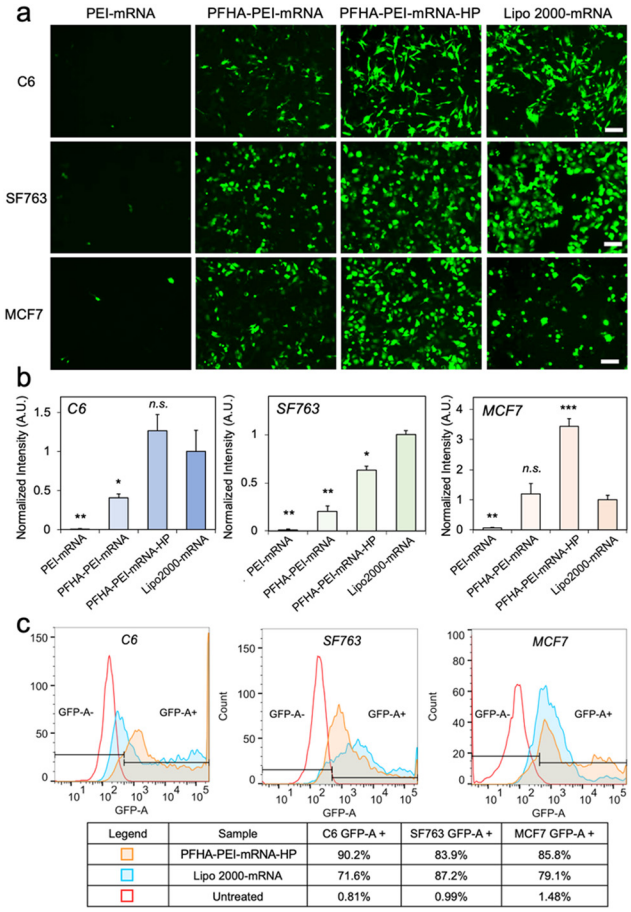

Legend	Sample	C6 GFP-A +	SF763 GFP-A +	MCF7 GFP-A +
	PFHA-PEI-mRNA-HP	90.2%	83.9%	85.8%
	Lipo 2000-mRNA	71.6%	87.2%	79.1%
	Untreated	0.81%	0.99%	1.48%

Fig. 6 Transfection results on three additional cancer cell lines. (a) Transfection images of PEI-mRNA, PFHA-PEI-mRNA and PFHA-PEI-mRNA-HP, with Lipofectamine 2000-mRNA as the positive control on C6, SF763 and MCF7 cells. Scale bar is 100 μm. (b) Quantitative analysis of the transfection results presented in (a). Statistical analysis was performed by comparing each of the treatment groups to the positive control Lipo2000-mRNA group. (c) Flow cytometric quantitative analysis of transfection efficiency of PFHA-PEI-mRNA-HP, with Lipofectamine 2000-mRNA as the positive control on the additional three cancer cell lines.

To test whether storing PFHA-PEI-mRNA-HP solution above 0 °C affects the stability and transfection functionality of mRNA, PFHA-PEI-mRNA-HP was refrigerated at 4 °C. Then, the PFHA-PEI-mRNA-HP samples stored at 4 °C were applied to 4T1 and HepG2 cells for transfection on day 0 (the same day the samples were prepared) as well as on day 1, day 2, day 3, day 4, day 7 and day 15 post-sample preparation. Lipofectamine 2000-mRNA was also prepared and stored and tested under similar conditions for comparison. The refrigerated PFHA-PEI-mRNA-HP and Lipofectamine 2000-mRNA samples were allowed to equilibrate to room temperature before they were applied to the cell culture each time. The results showed that PFHA-PEI-mRNA-HP stored at 4 °C did not show any significant compromise in transfection efficiency on both 4T1 and HepG2 cells for 15 days, indicating that mRNA was well-protected by the PFHA-PEI-HP construct and was able to maintain its structural stability and functionality for a prolonged period at 4 °C (Fig. 7a). On the other hand, Lipofectamine 2000-mRNA showed a significant decrease in transfection efficiency on both cell lines after just one day being stored at 4 °C. Lipofectamine 2000-mRNA lost most of its transfection efficiency after two days of refrigeration, suggesting that Lipofectamine 2000-mRNA is unstable when stored at 4 °C. Quantitatively, PFHA-PEI-mRNA-HP showed negligible loss of its transfection efficiency on 4T1 cells for 15 days, whereas Lipo-mRNA lost more than 70% of its transfection efficiency on day 1 and further lost 20%, causing its transfection efficiency to be only around 5% of that on day 0 between day 2 and 7 (Fig. 7b).

In the HepG2 cells, PFHA-PEI-mRNA-HP maintained 80% of its transfection efficiency even at day 15, even though its transfection efficiency fluctuated during the study, which could be due to the variation in the HepG2 conditions. On the other hand, Lipo-mRNA lost 90% of its transfection efficiency on HepG2 cells on day 1 and showed no recovery thereafter. Besides hydrolysis, a recent study also showed that the adduct formation between ionizable lipids and mRNA at temperatures above 0 °C could compromise the structural integrity of mRNA and cause suppressed protein experssion.[66] Since ionizable lipids are indispensable components in virtually all LNPs, the ionizable lipid-mRNA adduct formation could be one of the factors causing the quick decline in the functionality of Lipofectamine 2000-mRNA stored above 0 °C.

3.7 *In vitro* therapeutic mRNA delivery

To achieve therapeutic mRNA delivery, PFHA-PEI-HP was utilized to deliver IL12-encoding mRNA to 4T1 cells in a proof-of-principle study, with these cells later used in *in vivo* experiments. Interleukin-12 (IL12), a key cytokine secreted by monocytes and macrophages, is one of the pleiotropic cytokines modulating the potent activation pathways of essential immune cells such as natural killer (NK) cells, helper cells and cytotoxic T cells.[64] IL12 also establishes a positive feedback loop with other proinflammatory cytokines including tumor necrosis factor alpha (TNFa) and interferon gamma (IFNg), sustaining the cytotoxic functions of NK cells and T cells.[65]

To evaluate the efficacy of PFHA-PEI-mRNA-HP in delivering therapeutic IL12 mRNA, we encapsulated mouse IL12 mRNA within the nanoparticle system and treated 4T1 cells. As shown in Fig. 8a, immunofluorescence imaging 24 h post-treatment demonstrated strong IL-12 protein expression (red signal), while no IL-12 signal was detected in the untreated controls. The intense red fluorescence observed in the treated cells indicates the successful intracellular delivery and translation of the mRNA payload. Additionally, ELISA quantification of the secreted IL-12 protein in the culture medium confirmed a ~55-fold increase in IL-12 expression in the nanoparticle-treated cells compared to the untreated controls (Fig. 8b). These results demonstrate the high efficiency of PFHA-PEI-mRNA-HP in mediating functional mRNA delivery and cytokine production, highlighting its potential utility in cancer immunotherapy applications.

3.8 *In vivo* therapeutic efficacy and biosafety

Given its favorable physicochemical properties, high *in vitro* transfection efficiency, and robust storage stability, the

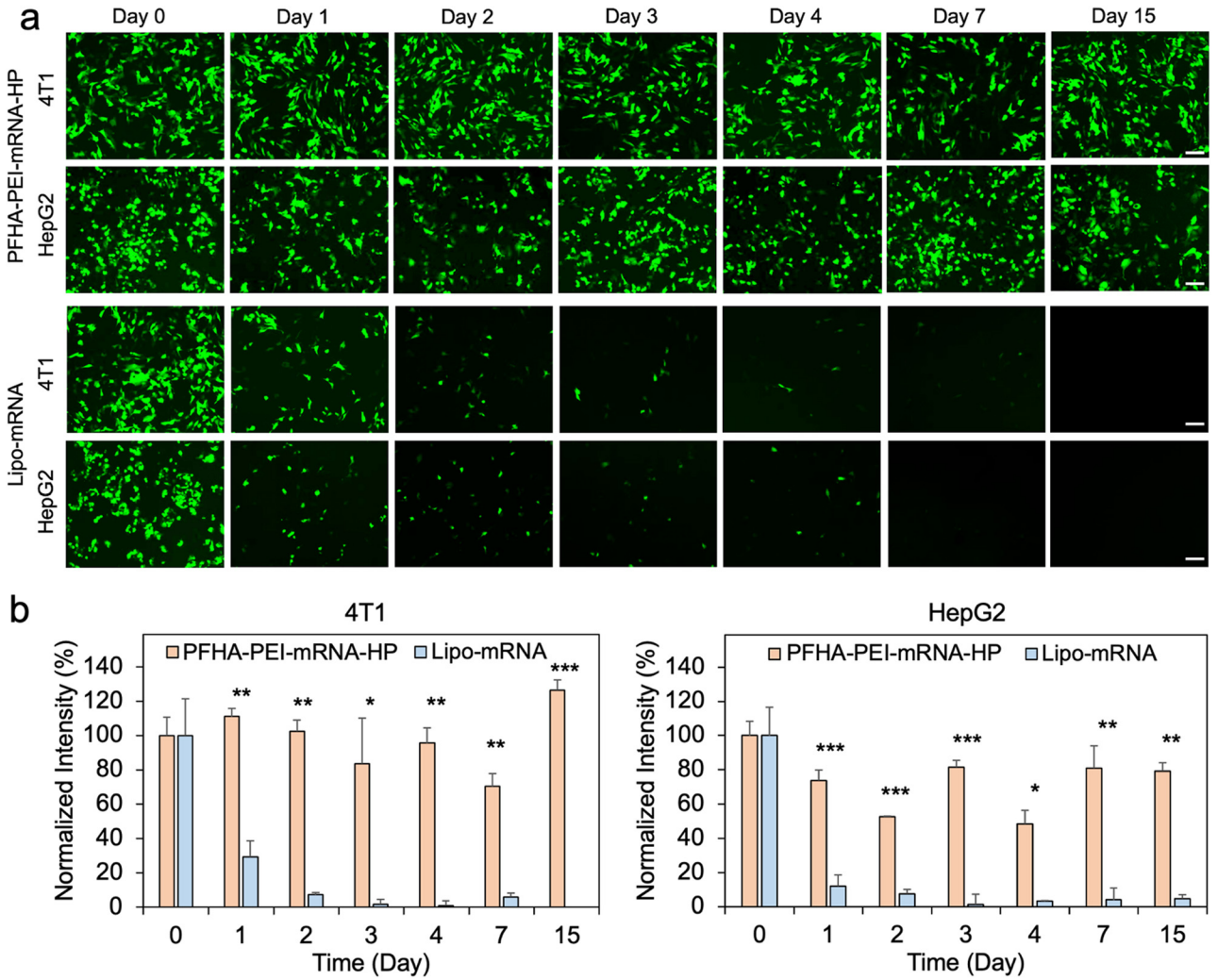

Fig. 7 Storage stability test above 0 °C on 4T1 and HepG2 cells. PFHA-PEI-mRNA-HP and Lipofectamine 2000-mRNA were prepared on day 0 and refrigerated at 4 °C throughout the course of the study. PFHA-PEI-mRNA-HP and Lipofectamine 2000-mRNA were allowed to equilibrate to room temperature before they were added to the 4T1 and HepG2 cell cultures at 2 μg mL^{-1} mRNA concentration on day 0, 1, 2, 3, 4, 7 and 15. (a) Fluorescent images of transfected cells. Images were collected 24 h after PFHA-PEI-mRNA-HP and Lipofectamine 2000-mRNA were added on each day. Scale bar is 100 μm. (b) Quantification of the fluorescence intensities shown in the images. Fluorescence intensities in each panel were normalized against the intensity at day 0, which was assigned as 100%.

PFHA-PEI-HP mRNA delivery system was evaluated for its *in vivo* therapeutic efficacy to explore its potential for clinical applications. This study utilized a 4T1 triple-negative breast cancer (TNBC) mouse model, which mimics the aggressive nature and treatment challenges of human TNBC, a subtype lacking estrogen, progesterone, and HER2 receptors, making it difficult to target with conventional therapies.[67,68]

Immunotherapy, particularly immune checkpoint inhibitors (ICIs), has shown promise for the treatment of TNBC by enhancing antitumor immunity by blocking inhibitory T-cell pathways. However, single-agent ICIs, such as anti-PD-L1 therapy, often exhibit limited efficacy in the immunosuppressive tumor microenvironment. Combining IL12 with anti-PD-L1 has been shown in preclinical studies to enhance anti-tumor immunity and overcome resistance to checkpoint blockade by promoting immune activation.

The 4T1 TNBC model, established by inoculating 4T1 cells into the mammary gland of BALB/c mice, was used due to its similarity to human TNBC, including rapid tumor growth, high metastatic potential, and an immunocompetent microenvironment. To confirm *in vivo* mRNA delivery, luciferase mRNA (luc mRNA) encapsulated in PFHA-PEI-HP nanoparticles was administered to BALB/c mice (Fig. 9a and b). To minimize mechanical disruption of the tumor and ensure close proximity for diffusion-based delivery, the nanoparticles were injected *via* peritumoral subcutaneous injection rather than intratumorally. This strategy has been adopted in other preclinical models for localized nanoparticle delivery and immunomodulation.[66,67] Four hours post-injection, the luminescence detected *via* IVIS imaging after luciferin administration confirmed successful mRNA transfection at the tumor site.

Following validation of IL12 mRNA delivery to 4T1 cells *in vitro* and mRNA (luc mRNA) delivery *in vivo*, the therapeutic

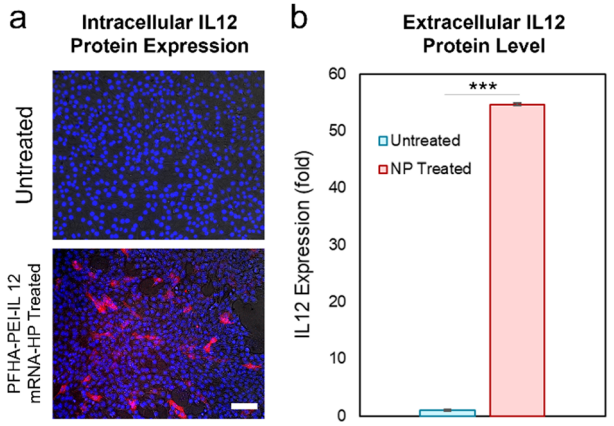

Fig. 8 IL12 mRNA delivery to 4T1 cells. (a) Immunofluorescence images showing IL-12 protein intracellular expression in 4T1 cell 24 h after treatment with PFHA-PEI-IL12 mRNA-HP nanoparticles (bottom) compared to untreated cells (top). Cells were stained with DAPI (blue, nuclei), and IL-12 protein was detected using an anti-IL-12 antibody (red). Scale bar is 100 μm. (b) Quantification of secreted IL-12 protein in culture medium *via* ELISA. PFHA-PEI-IL12 mRNA-HP nanoparticle-treated (NP treated) cells exhibited ~55-fold higher IL-12 expression compared to untreated controls. ***$p < 0.001$.

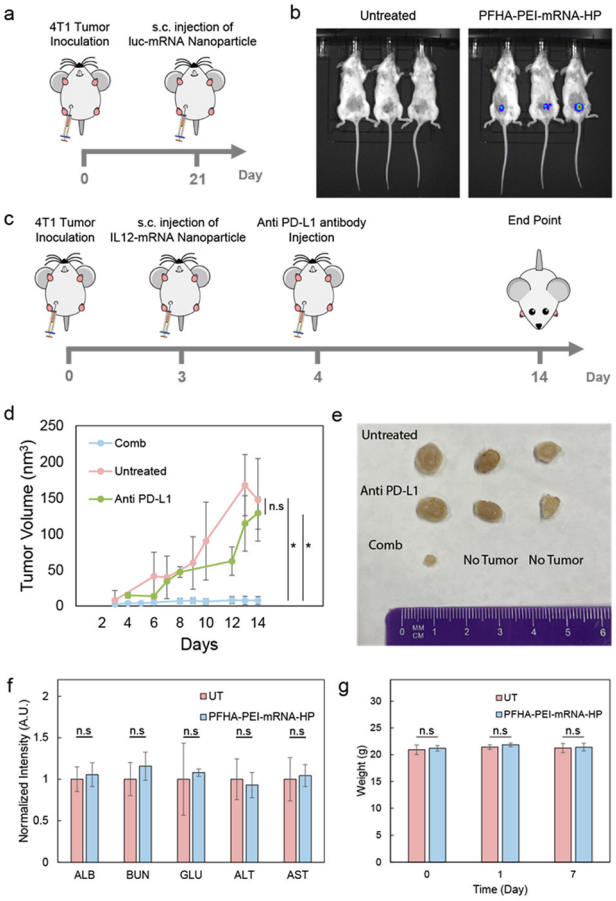

Fig. 9 *In vivo* therapeutic efficacy and biosafety of PFHA-PEI-mRNA-HP nanoparticles. (a) Diagram of the treatment schedule for the *in vivo* luciferase mRNA transfection study. (b) IVIS imaging of mice 5 h post-subcutaneous injection of PFHA-PEI-mRNA-HP nanoparticles containing 15 μg luciferase mRNA, with untreated mice as controls. (c) Diagram of the treatment schedule for the *in vivo* therapeutic study. (d) Tumor volume measurements in mice treated with anti-PD-L1 antibody, IL12 mRNA encapsulated in PFHA-PEI-mRNA-HP nanoparticles, or combination therapy, compared to the untreated controls. (e) Representative tumor images from different treatment groups on day 14. (f) Blood chemistry analysis of untreated and PFHA-PEI-mRNA-HP-treated mice. (g) Body weight monitoring of untreated and PFHA-PEI-mRNA-HP-treated mice over the treatment period, showing no significant weight loss.

potential of PFHA-PEI-HP was assessed by combining IL12 mRNA delivery with anti-PD-L1 therapy (referred to as "Comb" treatment). The treatment schedule (Fig. 9c) involved inoculating 4T1 cells on day 0, administering PFHA-PEI-HP with IL12 mRNA subcutaneously on day 3, and injecting anti-PD-L1 on day 4. The dosing regimen was selected based on preliminary internal studies to optimize the transfection efficiency, immune activation, and tolerability within a suitable time window. The control groups included anti-PD-L1-only and untreated mice. The tumor volume was monitored from day 3 to day 14 (Fig. 9d). The Comb group exhibited significant tumor suppression, with 4 of 6 mice tumor-free by day 14 and the remaining two showing minimal tumor growth (Fig. 9e). In contrast, the anti-PD-L1-only and untreated groups displayed substantial tumor progression.

Although marked tumor suppression was observed following treatment with PFHA-PEI-IL12 mRNA-HP and anti-PD-L1, IL-12 expression in the tumor tissues was not directly measured. However, the *in vitro* ELISA results (Fig. 8) confirmed strong IL-12 protein expression, and *in vivo* luciferase imaging (Fig. 9b) demonstrated the ability of this platform to deliver and express mRNA in tumors. These findings, alongside the observed tumor suppression, suggest that the antitumor effect was likely mediated by IL-12 expression. A further limitation is the lack of an IL-12-only control group, preventing a direct comparison of individual *versus* combined treatment effects. However, prior studies demonstrated the enhanced efficacy of IL-12 therapies with PD-L1 blockade, supporting our approach.[68,69] Additionally, treatment began early (day 3 post-inoculation) before tumors were fully established or vascularized, enabling the evaluation of the immunostimulatory and vaccine-like effects of IL-12 mRNA but potentially not reflecting the challenges of mature solid tumors. Future studies will incorporate IL-12 monotherapy and delayed treatment in advanced tumor models to clarify the role played by each component in the treatment efficacy in clinically relevant settings.

In addition, biosafety was evaluated through blood chemistry analysis and body weight monitoring. One day after PFHA-PEI-mRNA-HP treatment, the blood chemistry of the treated and untreated mice was comparable, with no significant differences observed in their albumin (ALB), blood urea nitrogen (BUN), glucose (GLU), alanine aminotransferase (ALT), and aspartate aminotransferase (AST) levels (Fig. 9f). Additionally, the Comb-treated mice maintained a stable body weight over two weeks compared to the tumor-free mice (Fig. 9g), indicating no observable systemic toxicity from PFHA-PEI-HP combined with anti-PD-L1.

These results highlight PFHA-PEI-mRNA-HP as a safe and effective platform for mRNA-based immunotherapy, enhancing checkpoint blockade therapy, while maintaining a favorable safety profile. This system shows significant promise for clinical translation in TNBC and other aggressive malignancies.

4. Conclusions

This study presented PFHA-PEI-mRNA-HP, a novel polymeric mRNA delivery platform that uniquely combines fluorination and heparinization to overcome the limitations of existing gene delivery systems. While fluorination and heparinization have individually enhanced DNA and siRNA delivery, their combined use for mRNA delivery in polymeric carriers is unprecedented. PFHA-PEI-mRNA-HP achieved an exceptional transfection efficiency (>90%) across multiple cancer cell lines, surpassing the commercial standard Lipofectamine 2000. The compact, spherical nanoparticles of the platform, enabled by PFHA, addressed the inability of PEI to effectively condense mRNA alone. Fluorination enhanced its cellular uptake through biphasic separation and bolstered its endosomal escape, while heparinization further improved its uptake, transfection efficiency, and biocompatibility. These well-balanced physicochemical properties, including compactness, cationic surface charge, and robust cellular internalization, underpinned its superior performance.

PFHA-PEI-mRNA-HP demonstrated remarkable versatility, seamlessly accommodating therapeutic mRNA and targeting ligands to enable precise therapeutic applications. *In vivo*, it efficiently delivered IL12 mRNA, and when combined with anti-PD-L1 therapy, achieved significant tumor suppression in a 4T1 triple-negative breast cancer (TNBC) mouse model. This combination therapy led to complete tumor regression in a subset of treated mice, highlighting its potent antitumor efficacy. Importantly, the platform maintained an excellent safety profile, with no observable toxicity, as evidenced by the stable body weight, normal blood chemistry, and absence of adverse effects in the treated animals. The synergistic effects of fluorination and heparinization not only enhanced its delivery efficiency but also ensured its compatibility with biological systems, making PFHA-PEI-mRNA-HP a robust candidate for clinical translation.

Furthermore, PFHA-PEI-mRNA-HP exhibited greater stability than Lipofectamine 2000 when stored above 0 °C, suggesting its potential for simplified storage and distribution. In conclusion, PFHA-PEI-mRNA-HP represents a highly efficient, stable, and versatile mRNA delivery platform with significant promise for cancer immunotherapy and broader gene therapy applications.

Author contributions

Conceptualization/validation/methodology/investigation, G. L., J. H., and M. Z.; formal analysis/data curation, G. L., J. H., X. L. and Y. L.; investigation, G. L., J. H., X. L., Y. L., T. J., A. F. and M. Z.; writing – original draft preparation, G. L. and J. H.; writing – review and editing, G. L., J. H. and M. Z.; supervision, M. Z. All authors have read and agreed to the published version of the manuscript.

Conflicts of interest

There are no conflicts of interest to declare.

Data availability

We confirm that all the relevant research data supporting the findings of this study are available within the manuscript and the electronic SI. No databases have been used, and no references to such databases are contained in the manuscript or SI.

It includes fluorescence microscopy images for optimization of polymer:mRNA and mRNA:heparin ratios, HPLC, Raman, and ^{19}F NMR data confirming polymer purity and structure, dynamic light scattering and zeta potential measurements, encapsulation efficiency studies, cellular uptake and endosomal escape imaging, transfection dose optimization, cytotoxicity evaluation *via* live/dead staining, and nanoparticle morphology by TEM. Additional mechanistic insights such as FGFR involvement in nanoparticle uptake are also provided. See DOI: **https://doi.org/10.1039/d5nh00299k**

Acknowledgements

The work was supported by the Kuni Foundation and NIH grant (R01EB026890). We acknowledge the use of the equipment on NP characterization from the Nanoengineering and Science Institute and Molecular Engineering and Science Institute supported by NSF (NNCI-2025489, grant NNCI-1542101), the UW Department of Chemical Engineering (grant NIH S10 OD030224-01A1), the UW W. M. Keck Microscopy Center (grant S10OD016240) and the Department of Pathology's flow cytometry core facility.

References

1 K. A. Hajj and K. A. Whitehead, *Nat. Rev. Mater.*, 2017, **2**, 1–17.
2 P. S. Kowalski, A. Rudra, L. Miao and D. G. Anderson, *Mol. Ther.*, 2019, **27**, 710–728.
3 X. Hou, T. Zaks, R. Langer and Y. Dong, *Nat. Rev. Mater.*, 2021, **6**, 1094.
4 R. Tenchov, R. Bird, A. E. Curtze and Q. Zhou, *ACS Nano*, 2021, **15**, 16982–17015.
5 X. Huang, N. Kong, X. Zhang, Y. Cao, R. Langer and W. Tao, *Nat. Med.*, 2022, **28**, 2273–2287.
6 L. Schoenmaker, D. Witzigmann, J. A. Kulkarni, R. Verbeke, G. Kersten, W. Jiskoot and D. J. A. Crommelin, *Int. J. Pharm.*, 2021, **601**, 120586.
7 M. L. Brader, S. J. Williams, J. M. Banks, W. H. Hui, Z. H. Zhou and L. Jin, *Biophys. J.*, 2021, **120**, 2766–2770.
8 M. Y. Arteta, T. Kjellman, S. Bartesaghi, S. Wallin, X. Wu, A. J. Kvist, A. Dabkowska, N. Székely, A. Radulescu, J. Bergenholtz

and L. Lindfors, *Proc. Natl. Acad. Sci. U. S. A.*, 2018, **115**, E3351–E3360.
9 E. Samaridou, J. Heyes and P. Lutwyche, *Adv. Drug Delivery Rev.*, 2020, **154–155**, 37–63.
10 J. Kim, Y. Eygeris, M. Gupta and G. Sahay, *Adv. Drug Delivery Rev.*, 2021, **170**, 83–112.
11 E. Kon, N. Ad-El, I. Hazan-Halevy, L. Stotsky-Oterin and D. Peer, *Nat. Rev. Clin. Oncol.*, 2023, **20**, 739–754.
12 S. S. Nogueira, A. Schlegel, K. Maxeiner, B. Weber, M. Barz, M. A. Schroer, C. E. Blanchet, D. I. Svergun, S. Ramishetti, D. Peer, P. Langguth, U. Sahin and H. Haas, *ACS Appl. Nano Mater.*, 2020, **3**, 10634–10645.
13 C. D. Siewert, H. Haas, V. Cornet, S. S. Nogueira, T. Nawroth, L. Uebbing, A. Ziller, J. Al-Gousous, A. Radulescu, M. A. Schroer, C. E. Blanchet, D. I. Svergun, M. P. Radsak, U. Sahin and P. Langguth, *Cells*, 2020, **9**, 2034.
14 S. Iqbal, M. Blenner, A. Alexander-Bryant and J. Larsen, *Biomacromolecules*, 2020, **21**, 1327–1350.
15 C. Zeng, C. Zhang, P. G. Walker and Y. Dong, *Lipid Nanoparticles for Delivery of mRNA Vaccines*, Springer Nature, 2020.
16 M. Zhao, M. Li, Z. Zhang, T. Gong and X. Sun, *Drug Delivery*, 2015, **23**, 2596–2607.
17 M. Li, M. Zhao, Y. Fu, Y. Li, T. Gong, Z. Zhang and X. Sun, *J. Controlled Release*, 2016, **228**, 9–19.
18 A. B. Vogel, L. Lambert, E. Kinnear, D. Busse, S. Erbar, K. C. Reuter, L. Wicke, M. Perkovic, T. Beissert, H. Haas, S. T. Reece, U. Sahin and J. S. Tregoning, *Mol. Ther.*, 2018, **26**, 446–455.
19 M. Chiper, N. Tounsi, R. Kole, A. Kichler and G. Zuber, *J. Controlled Release*, 2017, **246**, 60–70.
20 E. Lee, A. S. Kamlet, D. C. Powers, C. N. Neumann, G. B. Boursalian, T. Furuya, D. C. Choi, J. M. Hooker and T. Ritter, *Science*, 2011, **334**, 639–642.
21 Y. Takaoka, T. Sakamoto, S. Tsukiji, M. Narazaki, T. Matsuda, H. Tochio, M. Shirakawa and I. Hamachi, *Nat. Chem.*, 2009, **1**, 557–561.
22 Y. Wang, W. C. Lee, K. K. Manga, P. K. Ang, J. Lu, Y. P. Liu, C. T. Lim and K. P. Loh, *Adv. Mater.*, 2012, **24**, 4285–4290.
23 W. Liu, X. Huang, M. J. Cheng, R. J. Nielsen, W. A. Goddard and J. T. Groves, *Science*, 2012, **337**, 1322–1325.
24 M. Wang, H. Liu, L. Li and Y. Cheng, *Nat. Commun.*, 2014, **5**, 1–8.
25 G. Zuo, A. Xie, X. Pan, T. Su, J. Li and W. Dong, *ACS Appl. Nano Mater.*, 2018, **1**, 2376–2385.
26 H. Wang, Y. Wang, Y. Wang, J. Hu, T. Li, H. Liu, Q. Zhang and Y. Cheng, *Angew. Chem.*, 2015, **127**, 11813–11817.
27 Y. P. Xiao, J. Zhang, Y. H. Liu, J. H. Zhang, Q. Y. Yu, Z. Huang and X. Q. Yu, *Eur. J. Med. Chem.*, 2019, **162**, 602–611.
28 I. T. Horváth and J. Rábai, *Science*, 1994, **266**, 72–75.
29 M. C. Z. Kasuya, S. Nakano, R. Katayama and K. Hatanaka, *J. Fluorine Chem.*, 2011, **132**, 202–206.
30 M. P. Krafft, *Adv. Drug Delivery Rev.*, 2001, **47**, 209–228.
31 L. H. Wang, D. C. Wu, H. X. Xu and Y. Z. You, *Angew. Chem., Int. Ed.*, 2016, **55**, 755–759.
32 T. Wu, L. Wang, S. Ding and Y. You, *Macromol. Biosci.*, 2017, **17**, 1700114.
33 S. D. Xiong, L. Li, J. Jiang, L. P. Tong, S. Wu, Z. S. Xu and P. K. Chu, *Biomaterials*, 2010, **31**, 2673–2685.
34 M. E. Johnson, J. Shon, B. M. Guan, J. P. Patterson, N. J. Oldenhuis, A. C. Eldredge, N. C. Gianneschi and Z. Guan, *Bioconjugate Chem.*, 2016, **27**, 1784–1788.
35 C. Ge, J. Yang, S. Duan, Y. Liu, F. Meng and L. Yin, *Nano Lett.*, 2020, **20**, 1738–1746.
36 Z. Zhang, W. Shen, J. Ling, Y. Yan, J. Hu and Y. Cheng, *Nat. Commun.*, 2018, **9**, 1–8.
37 M. Ahmed and R. Narain, *Biomaterials*, 2013, **34**, 4368–4376.
38 S. P. Strand, S. Lelu, N. K. Reitan, C. D. L. Davies, P. Artursson and K. M. Vårum, *Biomaterials*, 2010, **31**, 975–987.
39 I. Pilipenko, V. Korzhikov-Vlakh, V. Sharoyko, N. Zhang, M. Schäfer-Korting, E. Rühl, C. Zoschke and T. Tennikova, *Pharmaceutics*, 2018, **10**, 117.
40 W. S. Boyle, K. Senger, J. Tolar and T. M. Reineke, *Biomacromolecules*, 2017, **18**, 56–67.
41 O. Jeon, H. S. Yang, T. J. Lee and B. S. Kim, *J. Controlled Release*, 2008, **132**, 236–242.
42 H. Sung, J. Ferlay, R. L. Siegel, M. Laversanne, I. Soerjomataram, A. Jemal and F. Bray, *CA-Cancer J. Clin.*, 2021, **71**, 209–249.
43 K. M. Hotchkiss and J. H. Sampson, *J. Neuro-Oncol.*, 2021, **151**, 55–62.
44 D. Camdzic, R. A. Dickman and D. S. Aga, *J. Hazard. Mater. Lett.*, 2021, **2**, 100023.
45 E. Blanco, H. Shen and M. Ferrari, *Nat. Biotechnol.*, 2015, **33**, 941–951.
46 S. Patel, N. Ashwanikumar, E. Robinson, A. Duross, C. Sun, K. E. Murphy-Benenato, C. Mihai, Ö. Almarsson and G. Sahay, *Nano Lett.*, 2017, **17**, 5711–5718.
47 C. Fornaguera, M. Guerra-Rebollo, M. Á. Lázaro, C. Castells-Sala, O. Meca-Cortés, V. Ramos-Pérez, A. Cascante, N. Rubio, J. Blanco and S. Borrós, *Adv. Healthcare Mater.*, 2018, **7**, 1800335.
48 F. Cardarelli, L. Digiacomo, C. Marchini, A. Amici, F. Salomone, G. Fiume, A. Rossetta, E. Gratton, D. Pozzi and G. Caracciolo, *Sci. Rep.*, 2016, **6**, 1–8.
49 Q. Mu, G. Lin, M. Jeon, H. Wang, F. C. Chang, R. A. Revia, J. Yu and M. Zhang, *Mater. Today*, 2021, **50**, 149–169.
50 S. E. Stanton, E. Gad, E. Ramos, L. Corulli, J. Annis, J. Childs, H. Katayama, S. Hanash, J. Marks and M. L. Disis, *npj Breast Cancer*, 2021, **7**, 1–9.
51 V. A. Arzumanian, O. I. Kiseleva and E. V. Poverennaya, *Int. J. Mol. Sci.*, 2021, **22**, 13135.
52 J. D. Torres-Vanegas, J. Cifuentes, P. R. Puentes, V. Quezada, A. J. Garcia-Brand, J. C. Cruz and L. H. Reyes, *Front. Chem.*, 2022, **10**, 1169.
53 B. Smolková, T. MacCulloch, T. F. Rockwood, M. Liu, S. J. W. Henry, A. Frtús, M. Uzhytchak, M. Lunova, M. Hof, P. Jurkiewicz, A. Dejneka, N. Stephanopoulos and O. Lunov, *ACS Appl. Mater. Interfaces*, 2021, **13**, 46375–46390.

54 D. Pei and M. Buyanova, *Bioconjugate Chem.*, 2019, **30**, 273–283.
55 Z. He, K. Liu, E. Manaloto, A. Casey, G. P. Cribaro, H. J. Byrne, F. Tian, C. Barcia, G. E. Conway, P. J. Cullen and J. F. Curtin, *Sci. Rep.*, 2018, **8**, 1–11.
56 Y. Ping, Q. Hu, G. Tang and J. Li, *Biomaterials*, 2013, **34**, 6482–6494.
57 R. Porta, R. Borea, A. Coelho, S. Khan, A. Araújo, P. Reclusa, T. Franchina, N. Van Der Steen, P. Van Dam, J. Ferri, R. Sirera, A. Naing, D. Hong and C. Rolfo, *Crit. Rev. Oncol.*, 2017, **113**, 256–267.
58 L. Pellegrini, D. F. Burke, F. Von Delft, B. Mulloy and T. L. Blundell, *Nature*, 2000, **407**, 1029–1034.
59 R. F. Barth and B. Kaur, *J. Neuro-Oncol.*, 2009, **94**, 299–312.
60 A. V. Lee, S. Oesterreich and N. E. Davidson, *JNCI, J. Natl. Cancer Inst.*, 2015, **107**, 73.
61 X. Zheng, G. Shen, X. Yang and W. Liu, *Cancer Res.*, 2007, **67**, 3691–3697.
62 M. N. Uddin and M. A. Roni, *Vaccines*, 2021, **9**, 1033.
63 H. Muramatsu, K. Lam, C. Bajusz, D. Laczkó, K. Karikó, P. Schreiner, A. Martin, P. Lutwyche, J. Heyes and N. Pardi, *Mol. Ther.*, 2022, **30**, 1941–1951.
64 A. E. Barberio, S. G. Smith, I. S. Pires, S. Iyer, F. Reinhardt, M. B. Melo, H. Suh, R. A. Weinberg, D. J. Irvine and P. T. Hammond, *Bioeng. Transl. Med.*, 2023, **8**, e10453.
65 J. Hodge-Dufour, M. W. Marino, M. R. Horton, A. Jungbluth, M. D. Burdick, R. M. Strieter, P. W. Noble, C. A. Hunter and E. Puré, *Proc. Natl. Acad. Sci. U. S. A.*, 1998, **95**, 13806–13811.
66 H. Shen, Q. Gao, Q. Ye, S. Yang, Y. Wu, Q. Huang, X. Wang and Z. Sun, *Int. J. Nanomed.*, 2018, **13**, 7409–7426.
67 Q. G. Wright, D. Sinha, J. W. Wells, I. H. Frazer, J. L. Gonzalez Cruz and G. R. Leggatt, *J. Immunother Cancer*, 2024, 12.
68 J. Lakshmipathi, S. Santha, M. Li, Y. Qian, S. F. Roy, N. Luheshi, K. Politi, M. Bosenberg, J. Eyles and V. Muthusamy, *Cancer Immunol. Immunother.*, 2025, **74**, 250.
69 C. Xu, Y. Zhang, P. A. Rolfe, V. M. Hernández, W. Guzman, G. Kradjian, B. Marelli, G. Qin, J. Qi, H. Wang, H. Yu, R. Tighe, K. M. Lo, J. M. English, L. Radvanyi and Y. Lan, *Clin. Cancer Res.*, 2017, **23**, 5869–5880.

